**The Dissertation Committee for Yeon Ho Kim Certifies that this is
the approved version of the following dissertation:**

Ensemble and Single Molecules Fluorescence Studies of Polymers

Committee:

David A. Vanden Bout, Supervisor

Alan Campion

Jason B. Shear

Dmitrii E. Makarov

Thomas M. Truskett

Ensemble and Single Molecules Fluorescence Studies of Polymers

by

Yeon Ho Kim, B.S., M.S.

Dissertation

Presented to the Faculty of the Graduate School of

The University of Texas at Austin

in Partial Fulfillment

of the Requirements

for the Degree of

Doctor of Philosophy

The University of Texas at Austin

December, 2007

Dedication

To the Lord and my family

Acknowledgements

This dissertation owes thanks to the many people who helped me to get it into the form that you are reading now. First of all, I should thank Dr. David Vanden Bout for his patient mentorship and inspiration throughout the research at the graduate school. I also owe the current and previous members of the Vanden Bout group for this work. Especially, I would like to thank Joyce, who bore my existence and suffered the bittersweet fruit of intense graduate research with me while we were in the lab together. My good friends outside the lab should also be acknowledged for the times and passion they shared with me. I cannot put enough emphasis on the fact that this work would not be finished without my parents who are always my best supporters, and pray for me every day. My sisters, Ji-young and Ji-hye, are not an exception in the support and love for me, too. Last but not least, I thank my lovely wife, Ui Jeong for the trust, support and love she always provides to me readily.

Ensemble and Single Molecules Fluorescence Studies of Polymers

Publication No._____

Yeon Ho Kim, Ph.D.

The University of Texas at Austin, 2007

Supervisor: David A. Vanden Bout

The effects of chain conformation on the photo-oxidation and green emission of poly(9,9-dioctylfluorenyl-2,7-diyl) (PFO) are investigated at both single molecule and ensemble levels. Single molecule studies reveal the conformation of PFO chains to be more globular when cast from THF than from toluene. Intensity transients of single molecules show that the elongated molecules cast from toluene have more fluctuations due to a fewer number of emitting centers on the polymer. Photochemical degradation leads to intensity fluctuations for the elongated molecules, while the globular chains show monotonic decays. Emission spectra of the single molecules show that photochemical oxidation leads to reduction in the emission of the molecule with no change in the emission spectra. No green emission is detected for single molecules indicating that formation of emissive ketone defects occurs rarely. Ensemble studies show that molecule cast from THF develop some green emission upon photodegredation while those cast from toluene don't. The increase in green in the globular molecules suggests that interchain contacts are necessary for the photochemical formation of

emissive ketone defects in the PFO. All emission spectra of the aggregated and non-aggregated PFO during photooxidation are also analyzed by using a modified Franck-Condon progression model with an additional independent Gaussian component and fitting results from single PFO spectrum. While emission spectrum of single PFO molecule shows a good fitting result to the model, the other two bulk PFO films display needs to introduce an additional term for better fit. This additional independent Gaussian component implies that green emission comes from non-Franck-Condon process.

Rotational dynamics of poly(methyl acrylate) is investigated by single molecule spectroscopy. Polarized fluorescence transients from single rhodamine 6G dye embedded in polymer matrix above glass transition are analyzed and the correlation function of reduced linear dichroism is fit by a stretched exponential function. The fitting results suggest that non-exponential decay of correlation function. However, more rigorous study is needed because of the intrinsic statistical error of limited experimental data and the effect of high numerical objective.

Table of Contents

List of Figures

xi

Chapter 1:   Introduction and Dissertation Overview

INTRODUCTION TO SINGLE MOLECULE SPECTROSCOPY

Single molecule spectroscopy (SMS) is a technique used to investigate the properties of individual molecules that can be isolated from an ensemble.[1-7] It enables one to study distributions of properties that may be obscured in bulk or ensemble measurements, where the individual behavior cannot be distinguished and only average characteristics can be measured. Gas phase experiments, at ultra low vacuum, have been able to provide the similar information on the properties and dynamics of materials at single molecules levels for decades. However, in condensed phase, the idea of studying individual molecules is relatively new and the challenge has been to isolate the small single molecule signal form the background. Over the last 20 years, there have been dramatic improvement in photon detection technology[1-3] improved sensitivity, faster response time, and smaller dark counts. These new detectors have allowed single molecule techniques to expand in many fields of basic and applied sciences such as chemistry, physics, biology, material science, and biomedical engineering.

For the first SMS experiments, absorption techniques were used for detection.[8] These experiments relied on the very narrow absorption lines of materials at very low temperatures. By laser frequency-modulation (FM) spectroscopy,[9] the frequency of absorption on and off sharp resonance, the absorption of individual

molecules could be detected. Later, these techniques began to use fluorescence to investigate the system, and the sensitivity was greatly improved and it is most widely used currently. A major development in SMS was the move from low-temperature to room-temperature fluorescence techniques. The low-temperature method relied on very narrow frequency electronic transitions to isolate the molecules from each other. At room temperature, the electronic transitions are much too broad for this to work. Instead the molecules must be isolated by dilutions. This leads to two types of SMS at room temperature. In the first, a solution past through the focus of a laser beam and burst of fluorescence from single molecules were detected.[10-12] In a different experiment, the molecules were spatially isolated in a film and their positions imaged. The first such experiments limited the background from the matrix by exciting very small regions of the sample using near-field scanning microscopy, By limiting the excitation of the sample to spot < 100 nm, the signal of single molecule was significantly larger than the background.[13] Later, it was found that the NSOM tip generated a larger background than simply utilizing far-field optics and a high numerical aperture (NA) objective.[14,15] Since such methods have dominated SMS. The imaging methods offer an advantage over burst detection as the same molecule can be studied over time. Its spectrum, lifetime, and polarization can be measured to study how the molecule of its environment may be changing with time. Recently, many single molecule studies have moved from point excitation and detection with a single detector to wide-field excitation and image detection. This offers the advantage of studying many molecules simultaneously, but makes spectroscopic studies, e.g. spectra, polarizations, lifetimes, more challenging.

In SMS, a single fluorescent dye molecule is used to probe localized property such as biochemical kinetics, or polymer dynamics. This is why an important consideration in SMS is the right choice of fluorescent probe in SMS.
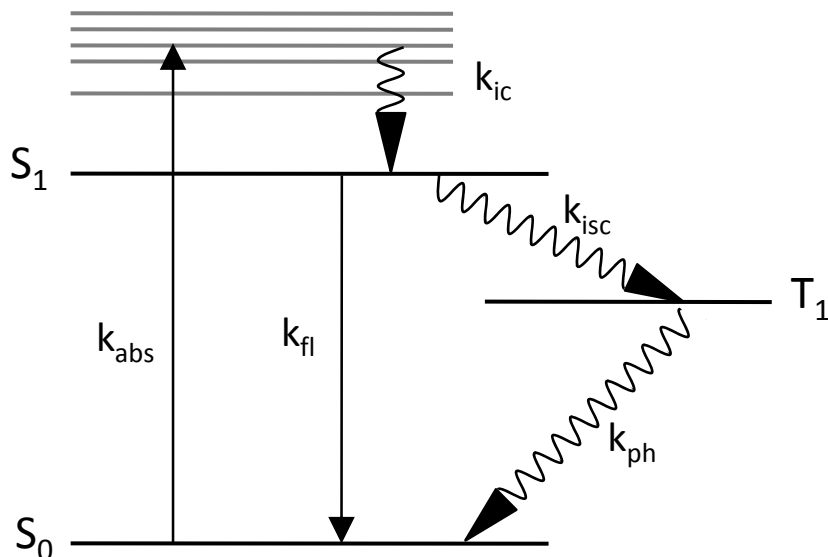
Figure 1.1: A simplified Jablonski diagram. See text for detailed explanation about the diagram

As seen in the Jablonski diagram[16] (Figure 1.1), a dye molecule at ground singlet state is transitioned to the excited singlet state when it gets absorption light of sufficient energy. The excited molecule experiences radiationless relaxation to the lowest electronic excited singlet states. The transition from S_1 to the ground states, S_0 is allowed resulting in fluorescence. The photon emission which occurs between different spin states ($T_1 \rightarrow S_0$) is termed phosphorescence. Because this process is "forbidden", it has a very slow rate and greatly reduced the SMS signal. When the molecule is in the triplet state, it is removed from the $S_0 \rightarrow S_1$ cycle to non-emissive. Single molecules can be detected by repeated excitation of the transition. At

3

saturation, the rate of emission will be limited by the radiative rate of the molecule. However, in general, the rate of emission is significantly lower. This is because while in the excited state, there is possibility of inter-system crossing (ISC) to the triplet state. As fluorescence is statistically much more likely than phosphorescence, the lifetimes of fluorescence is shorter ($1\times10^{-5} \sim 10^{-8}$ s) than phosphorescence (1×10^{-4}s $\sim$ minutes or hours). Therefore, to be a good candidate of probe in SMS, the probe must have a very small ISC lifetime rate so that a high quantum yield is achieved. A short excited state is also essential to maximize emission rate from S_1. In the ideal condition, the molecule would simply cycle between the ground states and excited singlet states emitting with every cycle continuously. When the spin state of excite state cross to the triplet from singlet, the molecule should stay at the triplet state for very short time and return to an emissive cycle as quickly as possible to improve the quality of the signal. Another important condition for an ideal probe in SMS is resistance to photochemical degradation such as photobleaching and photoblinking. This maximizes the total number of photons that can be detected and enables both better statistics as well as longer time studies.

How can the single molecule be confirmed in an experiment? Single molecules are well beyond the resolution of any optical method including NSOM. It is impossible to visualize the actual single molecule. In a SMS image, the size of the fluorescent spot for a single molecule is the size of the convolution of the laser focus and actual single molecule (essentially a delta function). There are a few ways to confirm if the data collected in the experiment is from a single molecule. First, in a scanned image, the number of bright spots of fluorescent single molecules should be proportional to the concentration of sample solution.

4
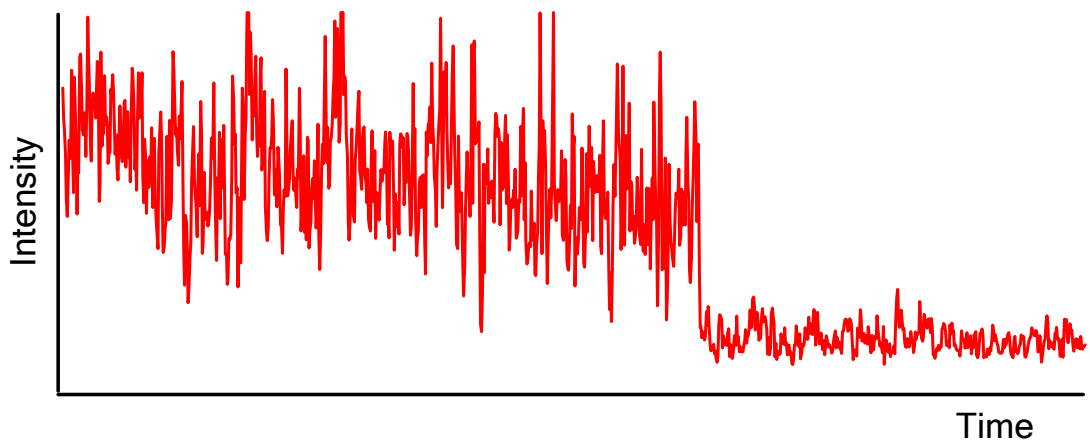
Figure 1.2: An example of single step photobleaching of a single Rhodamine 6G molecule at room temperature. Noise comes from the active dynamics of probe molecule at room temperature.

This excludes any possibility of aggregates. A single molecule should also have a well defined dipole moment. Therefore it should exhibit strong polarization contrast in both absorption and emission. Perhaps the most powerful method is to characterize the photobleaching. A fluorescent molecule is destroyed and loses its fluorescence after a long period of photon emission or irradiation of high power of excitation. The phenomenon is termed photobleaching and commonly observed in many fluorescent materials. A chromophore is defined the smallest unit of photo emitting. As singe probe dye molecule consists of single chromophore, the intensity of fluorescence from a single molecule is maintained constant (bright state). When the photobleaching of single dye molecule occurs, the molecule will lose its total fluorescence and the intensity instantly decreases to the background level in a single step. Photobleaching of mutichoromophore molecule displays monotonic decrease in total fluorescence intensity.

SINGLE MOLECULE SPECTROSCOPY IN CONJUGATE POLYMER

Conjugate polymers, or conductive polymer are of scientific and engineering interest because of their broad range of electronic device application such as organic emitting diodes (OLEDs), photovoltaic devices, thin film transistors, and chemical sensors.[17-32] Most conventional organic polymers report extremely high resistivity making them a good electronic insulators. In contrast, conjugate polymers[33] have delocalized bonds of π-electron conjugation that are half filled with electrons. This makes the materials behave like semiconductors. A number of polymeric systems have been synthesized for use as organic semiconductors. The derivatives of polymers such as poly(fluorene), poly(phenylene ethynylenes), and poly(phenylene vinylenes) account for most of studies of conjugate polymers. These materials have been adapted to have enhanced solubility in organic solvents and modified to have a wide variety of other optical and electrical properties.[34-37]

Many conjugate polymers have excited state species that emit efficiently in the visible range of the spectrum upon radiative relaxation, making them alternative for light emitting applications as well as photophysical characterization. Applications in the form of functional LEDs and thin film transistors and other photoconductive devices have been numerous in recent years.[22,24,38-42] However, the function of these devices is complicated by many factors. The conformation of the polymers can vary depending on processing conditions as well as their interchain contacts in the film. These differences in morphology lead to difference in the electronic and optical properties of the material. On top of this are the additional heterogeneities of the polydispersity of the polymer and potential chemical defects.

6
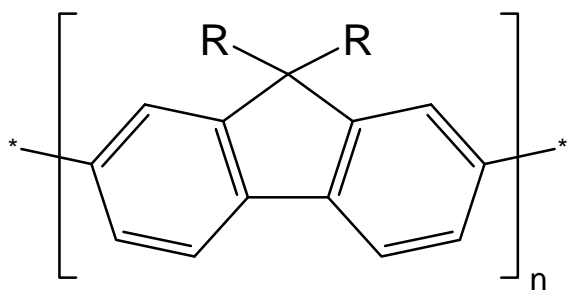
Poly(fluorene)
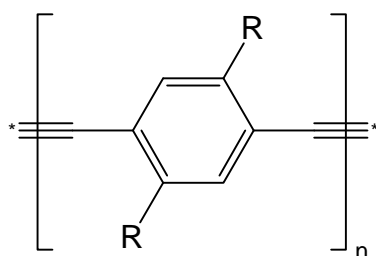
Poly(phenylene ethynylenes)
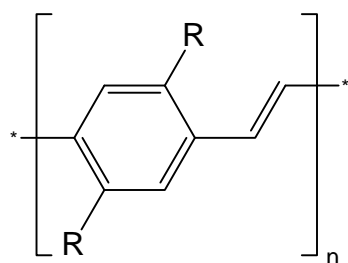
Poly(phenylene vinylenes)

Figure 1.3: Examples of conjugated polymer systems. Electron delocalization along the conjugated π-electrons of the backbone is possible due to the alternating π bonds.

All of these make such systems extremely difficult to characterize in the bulk. In many conjugate polymer systems, morphological and dynamical heterogeneity associated with chain-chain packing and complicated interactions among singlet, triplet excitons and charge species reciprocally play roles of photophysical character of conjugate polymers.[43] These nature of conjugate polymers make elaboration of their electronic and optical properties more difficult despite of relatively well defined excited state species. In addition, ordinary ensemble measure measurement of the properties often makes distribution of heterogeneous properties and makes it impossible to study an influence from one experimental condition exclusively.

In the context of these difficulties, single molecule spectroscopy (SMS) has been found to be a useful tool to expedite conjugate polymers.[44-61] One of the most notable single molecule study of conjugate polymer was reported in the work of poly(p-phenylene vinylene) (PPV) and poly(p-pyridylene vinylene) (PPyV) by Vanden Bout et. al.[44] It was reported that single molecules of conjugate polymer estimated to consist of over 1000 chromophores exhibit discrete intensity jumps by intramolecular electronic energy transfer. It enabled SMS to be used to access many processes of conjugate polymer systems, as any single molecule of conjugate polymer of a few hundred or thousand chromophore can be treated as a single system There have been many studies about what mechanism causes these conjugate polymers to behave like a single quantum system.[49,54,61,62] Poly[2-methoxy-5-(2'-ethyl-hexyloxy)-1,4-phenylenevinylene] (MEH-PPV) has been very well investigated and many great understanding has been brought to us via SMS.[45-48,54,56-58,61] By investigating one single conjugate polymer molecule at a time combined with microscope and/or spectrometer, researchers have been able to acquire spectral data and kinetic data that

are not obscured by sample heterogeneity. Single molecule modulation spectroscopy was developed and expanded to the field of investigation of triplet-triplet and singlet-triplet interaction of excited single conjugate polymer.[54,58] Single molecule polarization spectroscopy with theoretical calculation provides deeper insights in the chain conformation without interaction of other neighboring conjugate polymer chains.[63]

SMS study of polyfluorene conjugate polymer has been reported recently as well, mostly focusing on the appearance of its green band of emission spectra.[59,60] As one of the big questions regarding polyfluorene is whether interchain interaction causes the appearance of green band in its spectrum, SMS provides a novel method in elucidating the problem. For example, in the work of Becker *et. al.*,[60] emission spectra of single molecule of fluorene/fluorenone copolymer were investigated to monitor the intensity of green emission with respect to the increasing concentration of fluorenone on the polyfluorene chains. They demonstrated that the green emission scales linearly with fluorenone monomer and that the emission of defect can be excited by direct absorption. The conclusion of these studies is that the ketone sites alone are sufficient for generation of green emission and that interchain species such as excimers can be rigorously excluded.

Rising above technical difficulties at early age, SMS have been developed and applied to study molecular structure, and device physics of conjugate polymer single molecules. While many properties of conjugate polymer used to be buried by the shadow of ensemble averaging, the results of SMS has provided new insights in many subjects of conjugate polymer system such as morphological impact on photodynamics and spectroscopy and complex interactions among singlet exciton,

triplet excitons and holed polarons and so on. The experiments will offer the most possibility in a new level of understanding many processes inside conjugate polymers, which reserves big possibilities in many applications as well.

POLYMER DYNAMICS NEAR GLASS TRANSITION TEMPERATURE

Upon heating or cooling, a physical property of a material changes depending on its property. Amorphous materials show different characteristics than crystalline material. One of them is intuitively exemplified by variables, a specific volume and temperature (Figure 1.4(a)). Specific volume means volume per unit mass, ie, m^3/kg in SI (and MKS) units. The word specifically means 'per unit of mass' as distinct from "per mole". Most materials experience decreasing specific volume with declining temperature. At a temperature, there is a stark drop in specific volume followed by a distinct decrease in the rate of decline of specific volume with decline in temperature, which happens only in crystalline materials. This temperature is defined as a melting temperature (B) of a material, T_m. The material has a phase of liquid (A) above T_m, but a phase of solid (C) below T_m. By contrast, amorphous material has a region in which it shows only a change in the rate of decline of specific volume with decline in temperature instead of a stark drop. The temperature at which two asymptotic cooling curves meet is defined as a glass transition temperature of a material, T_g. The phase of material above a glass transition temperature but below a melting temperature is a supercooled liquid (D) and the material has a phase of glass (E) below a glass transition temperature.[64-66]

10

(a)

(b)

(c)
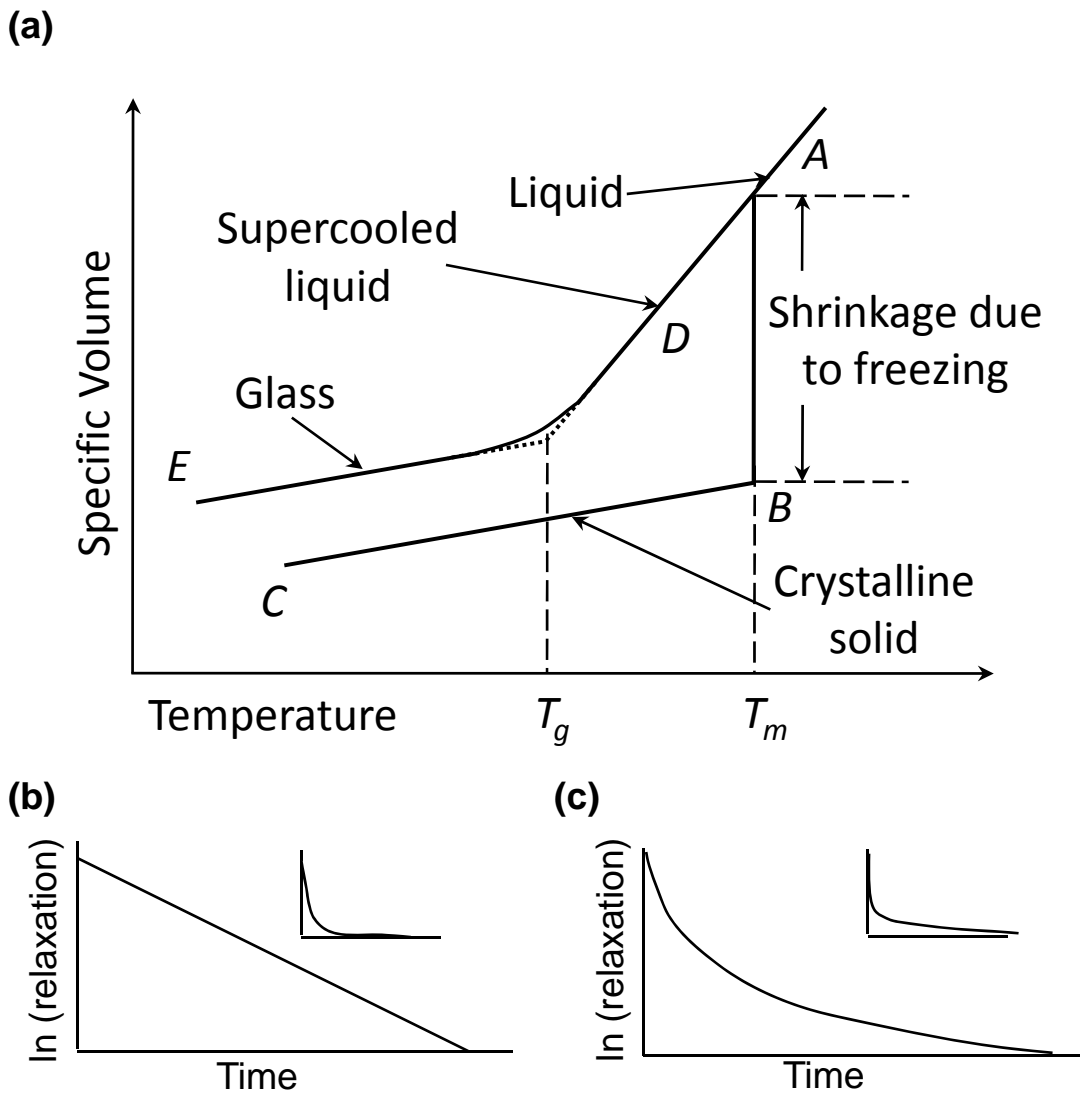
Figure 1.4: Phase diagram and dynamics relaxation curve of a material. **(a)** Thermodynamic properties of a crystalline or an amorphous material. A relaxation of the dynamics of the material could be either **(b)** single exponential decay or **(c)** multiple exponential decay depending on the temperature of the material.

In a liquid phase, molecules of a material move fast and almost freely. As temperature decreases, the movements of molecules become slower and the material experiences either freezing into solid or changing into supercooled liquid. All movements of molecules in solid phase are almost fixed and frozen. However, molecules in supercooled liquid phase can move but more slowly than those in liquid phase. As a supercooled liquid is cooled to a lower temperature, its density and viscosity increase but the specific volume decreases, and the molecules that comprise it move more and more slowly. At some temperature, i.e. a glass temperature, the molecules move so slowly that they do not have a chance to rearrange significantly before the temperature is further lowered. As these rearrangements are necessary for the material to find an equilibrium volume for that temperature, the experimentally observed properties of the material will begin to deviate from the equilibrium values at a given temperature. The specific volume is one of those properties as plotted in figure 1.4(a). The slope of the cooling curve below the glass transition temperature changes and the change rate becomes slower than when it is a supercooled liquid. As a result, a material exhibits different scales of dynamics depending on temperatures and whether it is an amorphous or a crystalline material. One of the most straightforward methods to probe and study the dynamics happening in a material is to investigate the rotation of a molecule doped into the material. Rotation of the molecules can be probed in a relatively easy way by monitoring the changes of polarizations of emission from the material. When molecules can freely move and rotate as in liquid phase, the polarization of emission from the material should be isotropic as rotation occurs before emission form the excited state. However, as the temperature decreases and the molecules of the material need more time and energy

12

to rotate or move to an equilibrium state, the change of polarization of emission from the material should be slower and less random than when it is in liquid phase. The time scale for relaxation can be characterized by the fluctuations in this polarization. The correlation function of the fluctuations yields a decay within the characteristic time scale. For Browinian motion, diffusion, this decay is a single exponential. Most polymer systems near T_g exhibit non-exponenetial decays. When the relaxation of a dynamics is measured and plotted with time, it tends to exhibit a single exponential decay (Figure 1.2(b)) in fast dynamics, but a multiple exponential decay or non-exponential decay in slower dynamics (Figure 1.2(c)).[64-74] the origin of this non-exponential decay has been of interest. SMS can be used to measure rotational dynamics of individual molecule and compare them to the ensemble.

In many cases of non-fluorescent polymer films, a fluorescent probe can be embedded in the polymer and make it possible to monitor the polarization changes attributing to dynamics. Single molecule spectroscopy (SMS) of an emissive probe embedded in polymer films provides a powerful tool to investigate the dynamics occurring in the polymer.[75-79] Whether the autocorrelation of polarized fluorescence signals from a probe is non-exponential or exponential gives a measure of rotational dynamics of the polymer. Especially, the capability of SMS to probe a microscopic domain of the polymer film can also open the possibility of enlightening the origin of macroscopic non-exponential or exponential dynamics.

DISSERTATION OVERVIEW

13

This work describes understanding the properties of polymer by the approach of single molecule spectroscopy, but is not limited to it. Emission property of polyfluorene is investigated with focusing on the green emission. Non-exponential decay of rotational dynamics relaxation is investigated using single molecule spectroscopy of probe molecules embedded in polymer matrix.

Chapter 1: Introduction and Dissertation Overview

The main purpose of this chapter is to familiarize readers to single molecule spectroscopy and its applications in studying properties of polymers. As referred by its name, single molecules spectroscopy is a powerful tool to investigate a chemical system without averaging distributions in the ensemble. The basic principle of single molecule spectroscopy and condition of a right dye probe for single molecule spectroscopy is explained for general introduction. A short presentation of conjugate polymers and single molecule study of the conjugate polymers is followed. Another section of introduction of polymer dynamics with respect to temperature is presented. Brief overviews of all the chapters are also included in this chapter.

Chapter 2: The Effects of Photochemical Oxidation and Chain Conformation on Green Emission of Poly(9,9-dioctylfluorene)

The origin of the green emission of polyfluorene and its derivatives has been discussed widely in many research groups and many greater understanding have been brought to us. However, our limitation still exists in whether a chain interaction or oxidation of polyfluorene chain causes green emission.[80-89] In this chapter, the emission spectra of poly(9,9-dioctylfluorenyl-2,7-diyl) is examined with an

emphasis on the appearance of green emission during photochemical oxidation both at single molecule and ensemble levels. Successive collection of emission spectra is performed to monitor the change of green emission during photochemical oxidation. In addition, the effects of chain conformation of PFO, which is controlled by solvent and confirmed by investigating polarization of fluorescence, on green emission is also presented to ensure the findings in this study. The findings suggest that defects generated by photochemical oxidation is not necessarily efficient emissive defect of green emission, but interchain   interaction enhances more green emission upon photobleaching.

Chapter 3: Photochemistry of Aggregated and Non-aggregated Polyfluorene: Huang-Rhys Parameter Analysis

Conjugate polymers, as referred by their name, have conjugated π-electrons along their backbone, which helps the excited electronic structure better defined. It is these π-electrons make conjugate polymers have unique properties different from other polymers. It is well known that Franck-Condon progression model works very well in such well defined systems.[90,91] The Huang-Rhys parameter analysis[92,93] which utilizes the Franck-Condon progression model provides more insightful information on conjugation of polymers. A modified Franck-Condon progression model, which includes an additiontial independent component, is used to explain different characteristics of polyfluorene. The comparison of Huang-Rhys parameters between emission spectra of aggregated polyfluorene and those of non-aggregated polyfluorene during photooxidation is presented to explain the difference of photochemistry between two conditions.

Chapter 4: Single Molecule Studies of Non-exponentiality of Rotation Dynamics of Rhodamine6G in Poly(methyl acrylate) matrix

Non-exponential characteristics[64-67,70,71] of rotational dynamics of a supercooled amorphous material have remained chanllenging problem for decades, while the single exponential decay of dynamics relaxation of normal liquid is well explained by Brownian diffusional model. The study of dynamics of a supercooled glass forming polymer, poly(methyl acrylate) (PMA), above its glass transition temperature is presented in this chapter. As PMA is non-fluorescent at the excitation of 533 nm, Rhodamine 6G single dye molecues are embedded in the PMA thin film matrix. Using polarization modulation and polarizing beamsplitter, the information of rotation is extracted to be analyzed by calculating reduced linear dichroism. For the analysis purpose, correlation function of the reduced linear dichroism is calculated and fitted to a stretched exponential for comparison. The resulting findings are discussed from the approaches of exponentiality and heterogeneity of monitored dynamics of single probe molecule.

REFERENCES

(1)   Basché, T. *Single-molecule optical detection, imaging and spectroscopy*; VCH: Cambridge, 1997.

(2)   Moerner, W. E.; Fromm, D. P. *Rev. Sci. Instrum.* **2003**, *74*, 2597.

(3)   Zander, C.; Enderlein, J.; Keller, R. A. **2002**.

(4)   Plakhotnik, T.; Donley, E. A.; Wild, U. P. *Annu. Rev. Phys. Chem.* **1997**, *48*, 181.

(5)   Weiss, S. *Science* **1999**, *283*, 1676.

(6)   Barbara, P. F. *Acc. Chem. Res.* **2005**, *38*, 503.

(7)   Xie, X. S.; Trautman, J. K. *Annu. Rev. Phys. Chem.* **1998**, *49*, 441.

(8)   Moerner, W. E.; Carter, T. P. *Phys. Rev. Lett.* **1987**, *59*, 2705.

(9)   Bjorklund, G. C. *Opt. Lett.* **1980**, *5*, 15.

(10)   Nie, S.; Chiu, D. T.; Zare, R. N. *Science* **1994**, *266*, 1018.

(11)   Nie, S.; Zare, R. N. *Anal. Chem.* **1995**, *67*, 2849.

(12)   Nie, S. M.; Zare, R. N. *Ann. Rev. Biophys. Biomol. Struct.* **1997**, *26*, 567.

(13)   Bian, R. X.; Dunn, R. C.; Xie, X. S.; Leung, P. T. *Phys. Rev. Lett.* **1995**, *75*, 4772.

(14)   Macklin, J. J.; Trautman, J. K.; Harris, T. D.; Brus, L. E. *Science* **1996**, *272*, 255.

(15)   Macklin, J. K. T. a. J. J. *Chem. Phys.* **1996**, *205*, 221.

(16)   Lakowicz, J. R. *Principles of Fluorescence Spectroscopy* 3rd ed ed.; Springer: New York, 2006.

(17)   Adams, D. M.; Kerimo, J.; Liu, C.-Y.; Bard, A. J.; Barbara, P. F. *J. Phys. Chem. B* **2000**, *104*, 6728.

(18)   Brown, A. R.; Greenham, N. C.; Burroughes, J. H.; Bradley, D. D. C.; Friend, R. H.; Burn, P. L.; Kraft, A.; Holmes, A. B. *Chem. Phys. Lett.* **1992**, *200*, 46.

(19)   Burroughes, J. H.; Bradley, D. D. C.; Brown, A. R.; Marks, R. N.; Mackay, K.; Friend, R. H.; Burn, P. L.; Holmes, A. B. *Nature* **1990**, *347*, 539.

(20)   Cao, Y.; Yu, G.; Heeger, A. J. *Adv. Mater.* **1998**, *10*, 917.

17

(21)   Choo, D. J.; Talai, A.; Lee, Y. K.; Jang, J.; Park, S. H.; Huh, G.; Yoo, K. H.; Lee, Y. J. *Thin Solid Films* **2000**, *363*, 37.

(22)   Friend, R. H. *Synth. Met.* **1992**, *51*, 357.

(23)   Friend, R. H.; Gymer, R. W.; Holmes, A. B.; Burroughes, J. H.; Marks, R. N.; Taliani, C.; Bradley, D. D. C.; Dos Santos, D. A.; Bredas, J. L.; Logdlund, M.; Salaneck, W. R. *Nature* **1999**, *397*, 121.

(24)   Granstrom, M.; Petritsch, K.; Arias, A. C.; Lux, A.; Anderson, M. R.; Friend, R. H. *Nature* **1998**, *395*.

(25)   Greenham, N. C.; Moratti, S. C.; Bradley, D. D. C.; Friend, R. H.; Holmes, A. B. *Nature* **1993**, *365*, 628.

(26)   Liu, J.; Yijian, S.; Liping, M.; Yang, Y. *J. Appl. Phys.* **2000**, *88*, 605.

(27)   Martin, S. J.; Bradley, D. D. C.; Lane, P. A.; Mellor, H.; Burn, P. L. *Phys. Rev. B: Condens. Matter* **1999**, *59*, 15133.

(28)   McNeil, J. D.; O'Connor, D. B.; Barbara, P. F. *J. Chem. Phys.* **2000**, *112*, 7811.

(29)   Pschirer, N. G.; Miteva, T.; Evans, U.; Roberst, R. S.; Marshall, A. R.; Neher, D.; Myrick, M.; Bunz, U. H. F. *Chem. Mater.* **2001**, *13*, 2691.

(30)   Yu, G.; Pei, Q.; Heeger, A. J. *Appl. Phys. Lett.* **1997**, *70*, 934.

(31)   Hide, F.; Diazgarsia, M. A.; Schwartz, B. J.; Heeger, A. J. *Acc. Chem. Res.* **1997**, *30*, 430.

(32)   Wang, H. L.; MacDiarmid, A. G.; Wang, Y. Z.; Gebler, D. D.; Epstein, A. J. *Synth. Met.* **1996**, *78*, 33.

(33)   Chiang, C. K.; Fincher, C. R.; Jr., Y. W. P.; Heeger, A. J.; Shirakawa, H.; Louis, E. J.; Gau, S. C.; MacDiarmid, A. G. *Phys. Rev. Lett.* **1977**, *39*, 1098.

(34)   Babel, A.; Jenekhe, S. A. *Macromolecules* **2003**, *36*, 7759.

(35)   Harrison, N. T.; Hayes, G. R.; Phillips, R. T.; Friend, R. H. *Phys. Rev. Lett.* **1996**, *77*, 1881.

(36)   Lee, N. H.-S.; Chen, Z.-K.; Chua, S.-J.; Lai, Y.-H.; Huang, W. *Thin Solid Films* **2000**, *363*, 106.

(37)   Osterbacka, R.; Genevicius, K.; Pivrikas, A.; Juska, G.; Arlauskas, K.; Kreouzis, T.; Bradley, D. D. C.; Stubb, H. *Synth. Met.* **2003**, *139*, 811.

(38)   Bradley, D. D. C. *Synth. Met.* **1993**, *54*, 401.

(39)   Liu, J.; Shi, Y.; Yang, Y. *Appl. Phys. Lett.* **2001**, *79*, 578.

(40)   Liu, M. S.; Jiang, X.; Herguth, P.; Jen, A. K.-Y. *Chem. Mater.* **2001**, *13*, 3820.

(41)   Yu, G.; Zhang, C.; Heeger, A. J. *Appl. Phys. Lett.* **1994**, *64*, 1540.

(42)   Zhang, Y.; Hu, Y.; Chen, J.; Zhou, Q.; Ma, D. *J. Phys. D: Appl. Phys.* **2003**, *36*, 2006.

(43)   Moliton, A.; Hiorns, R. C. *Polym. Int.* **2004**, *53*, 1397.

(44)   Vanden Bout, D. A.; Yip, W.-T.; Hu, D.; Fu, D.-K.; Swager, T. M.; Barbara, P. F. *Science* **1997**, *277*, 1074.

(45)   Lee, Y. J.; Kim, D. Y.; Barbara, P. F. *J. Phys. Chem. B* **2006**, *110*, 9739.

(46)   Grey, J. K.; Kim, D. Y.; Donley, C. L.; Miller, W. L.; Kim, J. S.; Silva, C.; Friend, R. H.; Barbara, P. F. *J. Phys. Chem. B* **2006**, *110*, 18898.

(47)   Kim, D. Y.; Grey, J. K.; Barbara, P. F. *Synth. Met.* **2006**, *156*, 336.

(48)   Lee, Y. J.; Kim, D. Y.; Grey, J. K.; Barbara, P. F. *ChemPhysChem* **2005**, *6*, 2404.

(49)   Grey, J. K.; Kim, D. Y.; Lee, Y. J.; Gutierrez, J. J.; Luong, N.; Ferraris, J. P.; Barbara, P. F. *Angew. Chem., Int. Ed. Engl.* **2005**, *44*, 6207.

(50)   Lee, Y. J.; Park, S.-J.; Gesquiere, A. J.; Barbara, P. F. *Appl. Phys. Lett.* **2005**, *87*, 051906/1.

(51)   Barbara, P. F. *Acc. Chem. Res.* **2005**, *38*, 503.

(52)   Barbara, P. F.; Gesquiere, A. J.; Park, S.-J.; Lee, Y. J. *Acc. Chem. Res.* **2005**, *38*, 602.

(53)   Gesquiere, A. J.; Park, S.-J.; Barbara, P. F. *J. Am. Chem. Soc.* **2005**, *127*, 9556.

(54)   Gesquiere, A. J.; Lee, Y. J.; Yu, J.; Barbara, P. F. *J. Phys. Chem. B* **2005**, *109*, 12366.

(55)   Gesquiere, A. J.; Uwada, T.; Asahi, T.; Masuhara, H.; Barbara, P. F. *Nano Lett.* **2005**, *5*, 1321.

(56)   Yu, J.; Lammi, R.; Gesquiere, A. J.; Barbara, P. F. *J. Phys. Chem. B* **2005**, *109*, 10025.

(57)   Yu, Z.; Barbara, P. F. *J. Phys. Chem. B* **2004**, *108*, 11321.

19

(58)   Gesquiere, A. J.; Park, S.-J.; Barbara, P. F. *J. Phys. Chem. B* **2004**, *108*, 10301.

(59)   Becker, K.; Lupton, J. M. *J. Am. Chem. Soc.* **2005**, *127*, 7306.

(60)   Becker, K.; Lupton, J. M.; Feldmann, J.; Nehls, B. S.; Galbrecht, F.; Gao, D.; Scherf, U. *Adv. Funct. Mater.* **2006**, *16*, 364.

(61)   Hu, D.; Yu, J.; Barbara, P. F. *J. Am. Chem. Soc.* **1999**, *121*, 6936.

(62)   Huser, T.; Yan, M.; Rothberg, L. J. *Proc. Natl. Acad. Sci. U. S. A.* **2000**, *97*, 11187.

(63)   Hu, D.; Yu, J.; Wong, K.; Bagchl, B.; Rossky, P. J.; Barbara, P. F. *Nature* **2000**, *405*, 1030.

(64)   Ediger, M. D. *Ann. Rev. Phys. Chem* **2000**, *51*, 99.

(65)   Ediger, M. D.; Angell, C. A.; Nagel, S. R. *J. Phys. Chem.* **1996**, *100*, 13200.

(66)   Harrison, G. *The Dynamic Properties of Supercooled Liquids*; Academic Press: New York, 1976.

(67)   Arbe, A.; Colmenero, J.; Monkenbusch, M.; Richter, D. *Phys. Rev. Lett.* **1998**, *81*, 590.

(68)   Cicerone, M. T.; Blackburn, F. R.; Ediger, M. D. *Macromolecules* **1995**, *28*, 8224.

(69)   Cicerone, M. T.; Ediger, M. D. *J. Chem. Phys.* **1995**, *103*, 5684.

(70)   Heuer, A.; Spiess, H. W. *Phys. Rev. Lett.* **1999**, *82*, 1335.

(71)   Lubchenko, V.; Wolynes, P. G. *Annu. Rev. Phys. Chem.* **2007**, *58*, 235.

(72)   Richert, R. *J. Phys.: Condens. Matter* **2002**, *14*, R703.

(73)   Wang, C.-Y.; Ediger, M. D. *J. Chem. Phys.* **2000**, *112*, 6933.

(74)   Phillips, J. C. *Rep. Prog. Phys.* **1996**, *59*, 1133.

(75)   Bartko, A. P.; Xu, K.; M, D. R. *Phys. Rev. Lett.* **2002**, *89*, 026101.

(76)   Deschenes, L. A.; Vanden Bout, D. A. *J. Phys. Chem. B* **2002**, *106*, 11438.

(77)   Rosenberg, S. A.; Quinlan, M. E.; Forkey, J. N.; Goldman, Y. E. *Acc. Chem. Res.* **2005**, *38*, 583.

(78)   Wei, C.-Y. J.; Kim, Y. H.; Darst, R. K.; Rossky, P. J.; Vanden Bout, D. A. *Phys. Rev. Lett.* **2005**, *95*, 173001.

(79) Wei, C.-Y. J.; Lu, C.-Y.; Kim, Y. H.; Vanden Bout, D. A. *J. Fluoresc.* **2007**, *17*, In press.

(80) Aharon, E.; Albo, A.; Kalina, M.; Frey, G. L. *Adv. Funct. Mater.* **2006**, *16*, 980.

(81) Dias, F. B.; Maiti, M.; Hintschich, S., I.; Monkman, A. P. *J. Chem. Phys.* **2005**, *122*, 54904.

(82) Dias, F. B.; Pollock, S.; Hedley, G.; Plsson, L.-O.; Monkman, A.; Perepichka, I. I.; Perepichka, I. F.; Tavasli, M.; Bryce, M. R. *J. Phys. Chem. B* **2006**, *110*, 19329.

(83) Romaner, L.; Piok, T.; Gadermaier, C.; Guentner, R.; Scandiucci de Freitas, P.; Scherf, U.; Cerullo, G.; Lanzani, G.; List, E. J. W. *Synth. Met.* **2003**, *139*, 851.

(84) Romaner, L.; Pogantsch, A.; Scandiucci de Freitas, P.; Scherf, U.; Gaal, M.; Zojer, E.; List, E. J. W. *Adv. Funct. Mater.* **2003**, *13*, 597.

(85) Rozanski, L.; Cone, C.; Ostrowski, D.; Vanden Bout, D. A. *Macromolecules* **2007**, *40*, 4524.

(86) Sims, M.; Bradley, D. D. C.; Ariu, M.; Koeberg, M.; Asimakis, A.; Grell, M.; Lidzey, D. G. *Adv. Funct. Mater.* **2004**, *14*, 765.

(87) Takeda, N.; Asaoka, S.; Miller, J. R. *J. Am. Chem. Soc.* **2006**, *128*, 16073.

(88) Whitehead, K. S.; Grell, M.; Bradley, D. D. C.; Jandke, M.; Strohriegl, P. *Appl. Phys. Lett.* **2000**, *76*, 2946.

(89) Zhao, W.; Cao, T.; White, J. M. *Adv. Funct. Mater.* **2004**, *14*, 783.

(90) Asada, K.; Kobayashi, T.; Naito, H. *Thin Solid Films* **2006**, *499*, 192.

(91) Clark, J.; Silva, C.; Friend, R. H.; Spano, F. C. *Phys. Rev. Lett.* **2007**, *98*, 206406.

(92) Henderson, B.; Imbusch, G. F. *Optical spectroscopy of inorganic solids*; Oxford University Press: New York, 1989.

(93) Huang, K.; Rhys, A. *Proc. R. Soc. London, A* **1950**, *204*, 406.

Chapter 2: The Effects of Photochemical Oxidation and Chain Conformation on Green Emission of Poly(9,9-dioctylfluorene)

INTRODUCTION

The use of conjugated polymers in light emitting diodes has attracted wide interest from scientists and engineers since its initial demonstration over a decade ago.[1] A number of materials have been utilized to generate red, green, and blue emission for display technologies. Red and green materials have been the most prominent, with fewer materials exhibiting good characteristics in the blue.[2-4] As a class, polyfluorenes have shown excellent promise as blue light emitting materials. However, the blue emission from polyfluorene LEDs has been noted to degrade to include a green component.[5-13] The source of this green emission has been a matter of some controversy.[5-16] Initial experiments associated the emission with polymer order as the annealing the films were shown to increase the green emission.[13] However, later studies have definitely shown the new emission band is associated with oxidative defects on the polymer.[7,10-13,17-20] Specifically, the inclusion of ketone defects in the form of fluorenone moieties along the polymer backbone gives rise to the identical emission of that seen in the polymers with oxidative damage.[16,18,20,21] The specific role of the ketone defects is still a point of some contention. On the one hand, several studies claim that the ketone defects alone are sufficient to produce the green emission.[6,15,17,19,22] These studies looked at well-controlled fluorene/fluorenone copolymers with varying fractions of fluorenone. They demonstrated that the green

emission scales linearly with fluorenone monomer and that the emission of defect can be excited by direct absorption.[15,16,21] The conclusion of these studies is that the ketone sites alone are sufficient for generation of green emission and that interchain species such as excimers can be rigorously excluded. However, there are other studies that contest this description and specifically claim that interchain species are required to explain the origin of the green emission.[12-14] These studies have typically examined isolated PFO chains that underwent photochemical oxidative damage. In these cases, it was the lack of green emission upon oxidative damage in isolated molecules and the appearance of green emission in bulk materials upon photochemistry that leads to the conclusion that interchain contacts were required. In one study, an excimer species that results from two fluorenone defects is invoked as the origin of the green emission.[12,13] In another, the authors simply conclude that interchain interactions are required.[14]

The studies reaching different conclusions are inherently different. In one case, co-polymers with known amounts of fluorenone were studied. In the other, polyfluorene polymers were subjected to photochemistry that generated fluorenone defects, but that also generated other photochemical damage. One way to try to limit the role of interchain interaction is to examine the emission of single chains. There have been a number of recent studies of single conjugated polymer molecules to address such issues.[14,15,23-26] Recently, there has been a report of single molecule studies of polyfluorene/fluorenone co-polymers[15] Images of single PFO was taken by means of spectral selection using blue and green bandpass filters centered at 460 nm and 550 nm and intensities of single molecules in the images were counted. This study agreed with the other copolymer studies that the ketone defect alone was

sufficient to explain the green emission. Most importantly, the study showed that no green emission could be seen from the pure polyfluorene, but that polymers with fluorenone exhibited the green emission. As the fluorenone content increased the number of molecules with green emission was constant, but the amplitude of the green emission increased. This study will examine the other case, that of oxidative damage to single PFO chains. In particular, the emission spectra of both single chains and ensembles of chains are examined to study the appearance of the green emission that results from photochemistry. A confocal microscope equipped with spectrometer keeps track of real-time spectral changes in emission spectra of PFO single molecules during photochemical oxidation. The role of chain morphology and intrachain interactions is examined by studying molecules cast from different solvents.

EXPERIMENTAL SECTION

Poly(9,9-dioctylfluorenyl-2,7-diyl) (PFO) was purchased from American Dye Source, Inc. and used without further purification. Molecular weight of PFO ranged from 40 kDa ~ 120 kDa. Polystyrene was purchased from Aldrich and used without additional purification. PFO solution and polystyrene solution were prepared with either toluene or tetrahydrofuran (THF). As valid in many other single molecule experiement, the concentration of PFO was lowered to find well isolated PFO single chains in polystyrene (PS) matrix. Normal concentration for best results was about 1 nM. The main purpose of PS film matrix was to fix PFO single chains on sample slide, as the glass transition temperature of PS is well above the room temperature. The non-fluorescent property of PS at given excitation makes it a good material for

single molecule experiment. Thin films were prepared with a spin coater (Specialty Coating Systems Inc., Model P6204-A). PFO in PS solution was spun-cast onto a cover slip rotating at about 2000 rpm. After then, the coverslip was placed in vacuum seal container to evaporate solvent remaining in samples.

(a)

(b)
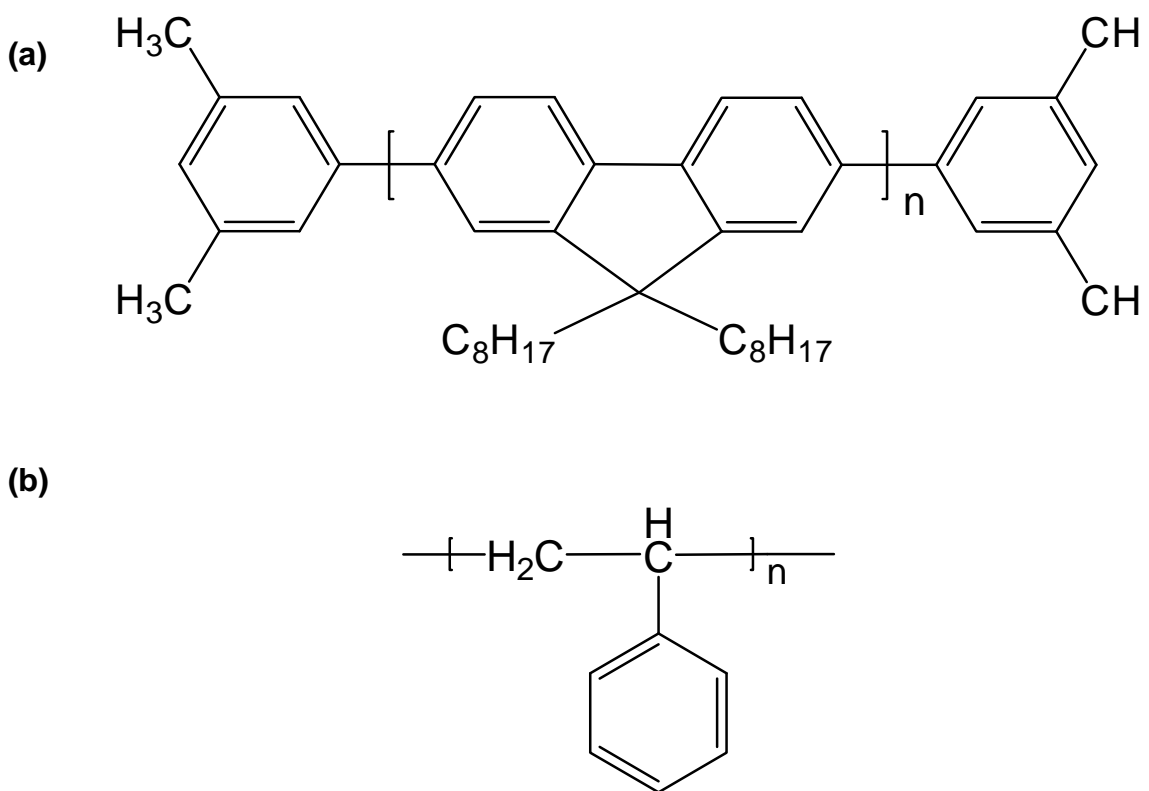
Figure 2.1: The chemical structures of **(a)** poly(9,9-dioctylfluorenyl-2,7-diyl) and **(b)** polystyrene.
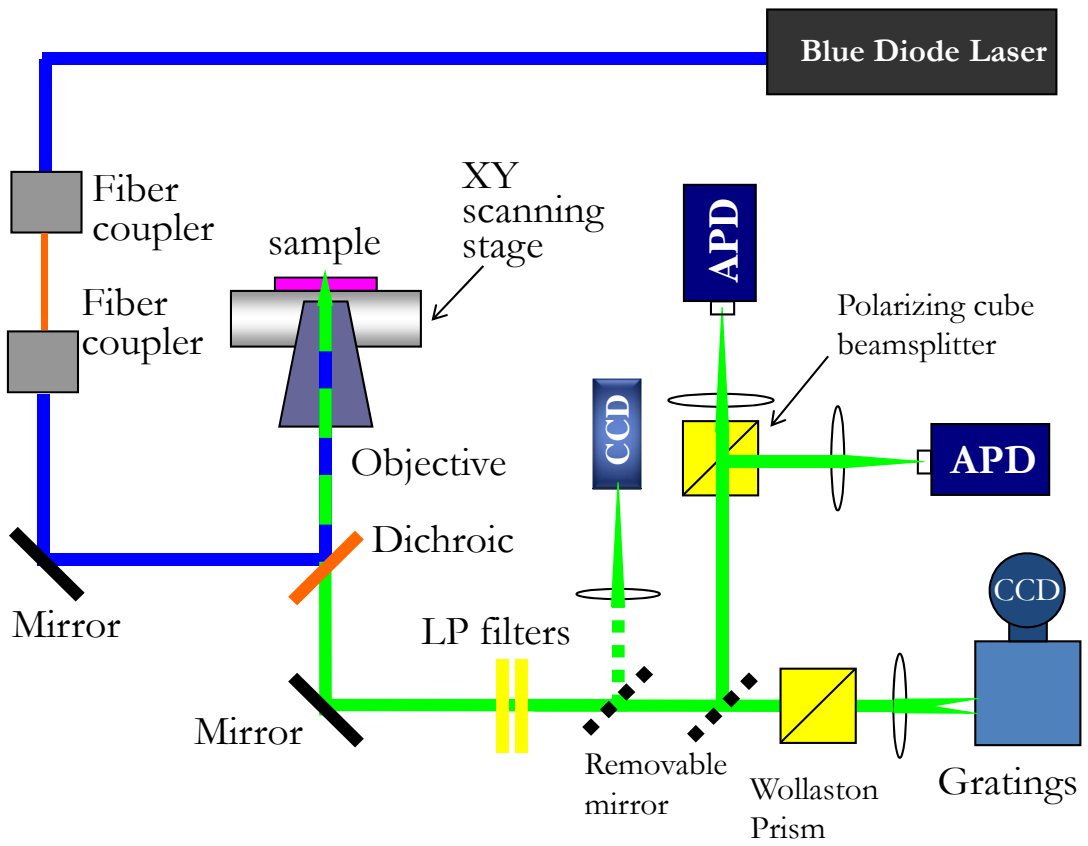
Figure 2.2: A simplified scheme of experimental setup for collecting emission spectra and transients of single PFO chains.

Experiments were performed using a home-built sample scanning inverted microscope as shown in figure 2.2. The samples were excited using a 405 nm CW laser (Coherent Auburn Division, Blue/violet Diode Laser System) by illuminating the sample off a dichroic mirror and through a 1.25 numerical aperture oil-immersion microscope objective in an epi configuration. The polarization of excitation beam was linear such that it was s-polarized with respect to the dichroic mirror. Laser power for scanning image was about 1.5 nW and laser power for probing ranged from about 0.015 μW to 1.5 μW. The sample fluorescence was collected through the same microscope objective and imaged either onto a single photon counting avalanche photodiode (SPCAPD) or onto a spectrometer (Acton) equipped with a CCD camera (Princeton Instruments, LN-400EB). The SPCAPD collected fluorescence over the time to display a time transient and the CCD was used to collect emission spectra of PFO. A polarized cube beamsplitter before two APDs was used to separate signals into two polarizations and a wollaston prism was placed before the spectrometer to separate and direct fluorescence of two orthogonal polarizations onto the CCD. The cube beamsplitter and the Wollaston prism provided information of chain conformation perceived in polarization. The Wollaston prism consists of two orthoganl calcite prism of perpendicular optic axes cemented together and results in having outgoing beam diverge from the prism, giving two polarized rays. The angle of divergence between two outgoing rays, which is 5º in the prism used in this work, is determined by the prisms' wedge angle and the wavelength of the light. It provides the advantage of collecting polarized spectra in one CCD detector as shown in figure 2.3. Single fluorescent chains were located in the sample by raster scanning the sample to generate a fluorescence image. Once located, individual chains were

centered in the excitation spot and transients recorded of their polarized emission spectra.
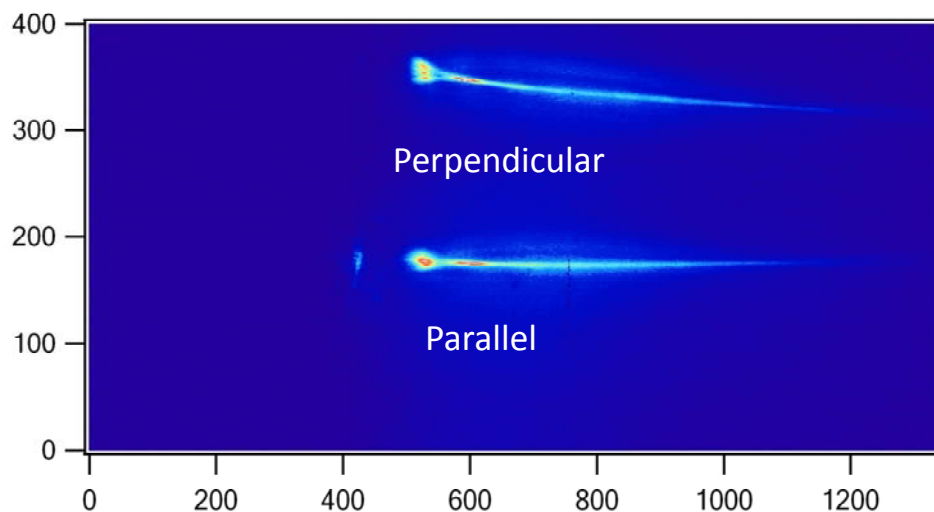
Figure 2.3: 2D image of polarized emission spectra of PFO after a Wollaston prism.

RESULTS AND DISCUSSION

Single Molecules Studies of Photochemistry

Figure 2.4 shows an example of an image of PFO chains isolated in a PS thin film cast from toluene. The excitation laser was linearly polarized in a direction that is vertical to the image direction. Figure 2.4(a) is the fluorescence that is polarized parallel to the excitation laser while figure 2.4(b) is the fluorescence that is polarized perpendicular to the laser excitation.

(a)　　　　　　　　　　**(b)**
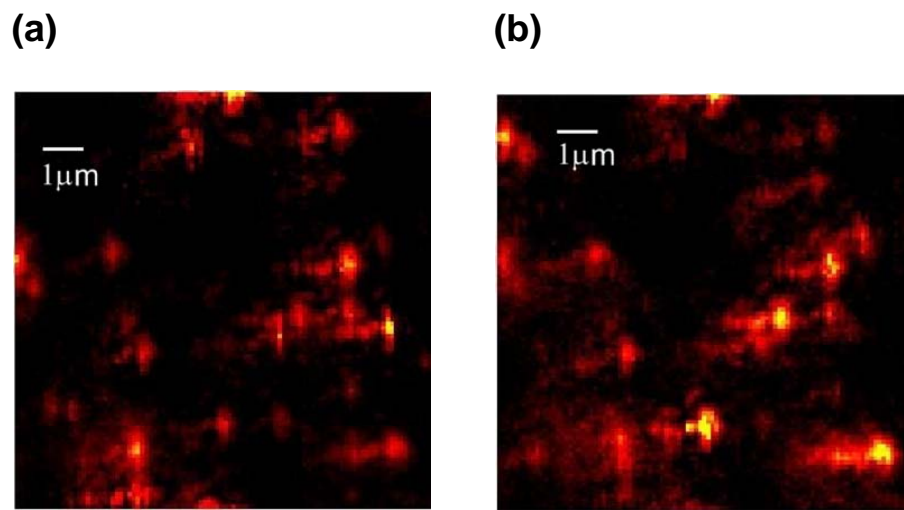
Figure 2.4: Microscopic fluorescence images of **(a)** parallel and **(b)** perpendicular
polarization of 10×10 μm scan of polystyrene film doped with well-
separated single PFO chains. The film was prepared by spin casting at
2000 rpm.

The variation in intensity in the spots results from their orientation with respect to the
excitation polarization as well as the polydispersity of the polymer sample. When one
of the PFO molecules is fixed in the laser focus and the fluorescence collected as a
function of time, the fluorescence transients exhibit very typical single molecule
behavior.[27-29] Figure 2.5 shows the transients of the parallel and perpendicular
polarizations of fluorescence from a single PFO molecule. The transient exhibits
discrete jumps in both intensity and polarization that would be expected from single
molecules (Figure 2.5(a)).[28] While this behavior is seen from many of the molecules,
others show more monotonic decays in intensity in both polarizations as shown in
figure 2.5(b). The characteristics of the transients are different depending on the
solvent the films are cast from.
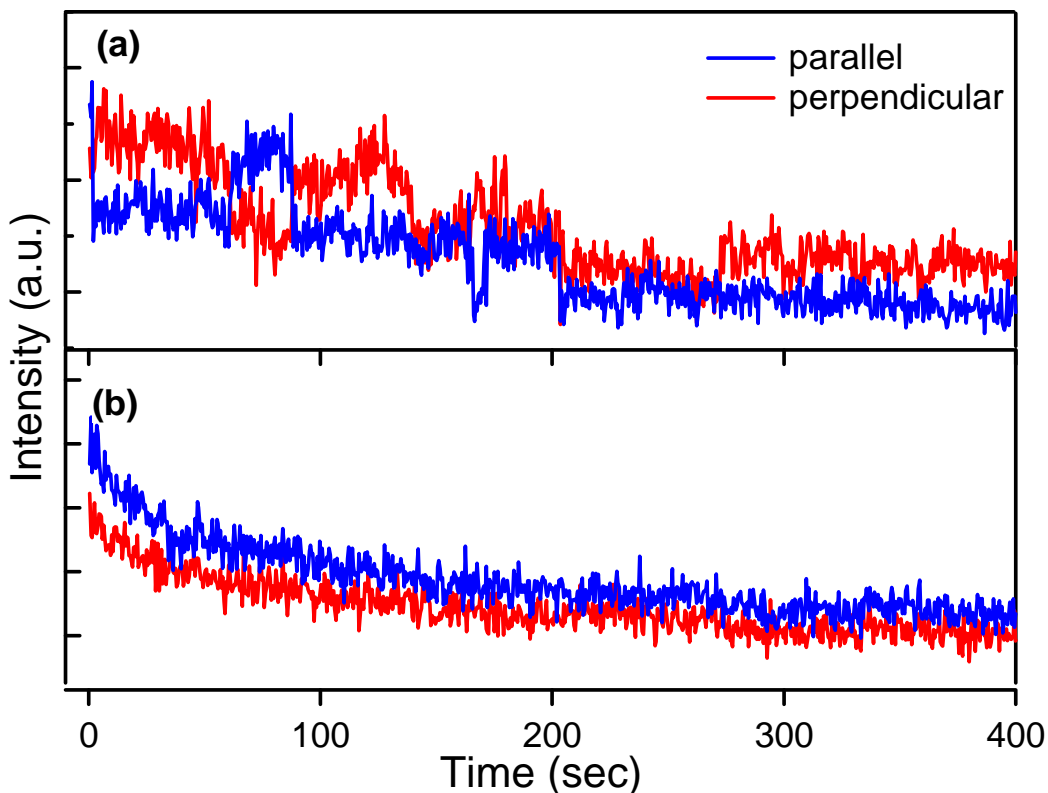
Figure 2.5: Fluorescence time-transients of single PFO chains collected with APD at two orthogonal directions. Single PFO chains exhibit **(a)** intensity jumps or **(b)** monotonic decays in fluorescence intensity.

Single PFO molecules cast from toluene show the full range of behaviors described above and more than half of single molecules analyzed exhibit discrete jumps in intensity as in figure 2.5(a), while >80% of PFO molecules cast from THF exhibit nearly monotonic decays in intensity with nearly unpolarized emission as in figure 2.5(b). Both the discrete jumps and eventual loss of fluorescence signals are the results of photochemistry.[30] The discrete jumps in the PFO molecules cast from toluene are indicative of energy transfer along the polymer chain to a specific emissive site. As this site is photobleached, the emission then originates from a new

30

point on the chain with potentially a different orientation. For the THF, the nearly isotropic emission is indicative of chain disorder to a collection of chromophores with an isotropic distribution.

Polarization of Emission from PFO Single Chains

The conformation of the polymer chain in the solution will be strongly influenced by the nature of the solvent. This conformation will be retained to some extent in films cast from the solution, particularly if the films are spin cast at a high speed where solvent evaporation proceeds more quickly than equilibration of the chain conformation.[25] These differences in conformation have been shown to affect both photo- and electro-luminescence properties of MEH-PPV thin films.[25] In the original work of Nguyen et. al. about polymer aggregate of MEH-PPV, an evidence was presented that the degree of interchain interaction and morphology is affected by controlling chain conformation and solvent used to prepare polymer solution has a good correlation with the conformation of polymer chain.[31] The chain conformations of MEH-PPV in different solvents were evidenced by light scattering, UV-Vis absorption and photoluminescence excitation spectra, luminescence quantum yield and exciton lifetime. It was reported that both concentration and solvents have impacts on the degree of aggregation. In their work, MEH-PPV chains showed much more extended and open conformation when chlorobenzene was used as a solvent. However, MEH-PPV chain showed tighter coil conformation when THF was used as a solvent.[31] Similar result is expected in polyfluorene chain conformation. In samples prepared using toluene as a solvent, the PFO chains are likely to have an extended conformation as toluene is a moderately good solvent for PFO, solvating primarily

the polymer backbone. In contrast, if THF is used as a solvent, the polymer will be less well solvated and is likely to adopt a collapsed globular structure, because THF is reported to solvate the side groups of polymer chains instead of the backbone. The conformation of PFO chains in films can be directly probed in the single molecule studies. The molecules are excited with linearly polarized light and the polarization of the emission is measured both parallel and perpendicular to the excitation. Single dye molecules show clear changes of intensity depending on their orientation, because there is one chromophore with a unique transition dipole direction. Understanding of the orientation of the polymer molecule by the method of polarization of fluorescence intensity is complicated because the polymers have many absorption chromophores and the chains can adopt a number of conformations.[32,33] In a previous study, the range of chain conformation of MEH-PPV was measured using Monte Carlo bead-on-a-chain simulations and single molecule polarization spectroscopy.[32] However, simple analysis of the emissions of single PFO molecules yields qualitative information about the structure of the chain as well as any energy transfer along the molecule. The values of polarization for individual molecules cast from both toluene and THF were measured and shown in figure 2.6. The intensity at the center of each fluorescence image of single PFO chain was used to calculate the polarization. The polarization values are the difference between the signals in two orthogonal polarizations normalized to total intensity. This will give a polarization value that ranges from -1 (perpendicular to the excitation) to +1 (parallel to the excitation). The molecules in toluene exhibit a broad distribution of linear dichroism ranging from molecules that have emission nearly perpendicular to the excitation to those almost perfectly parallel.
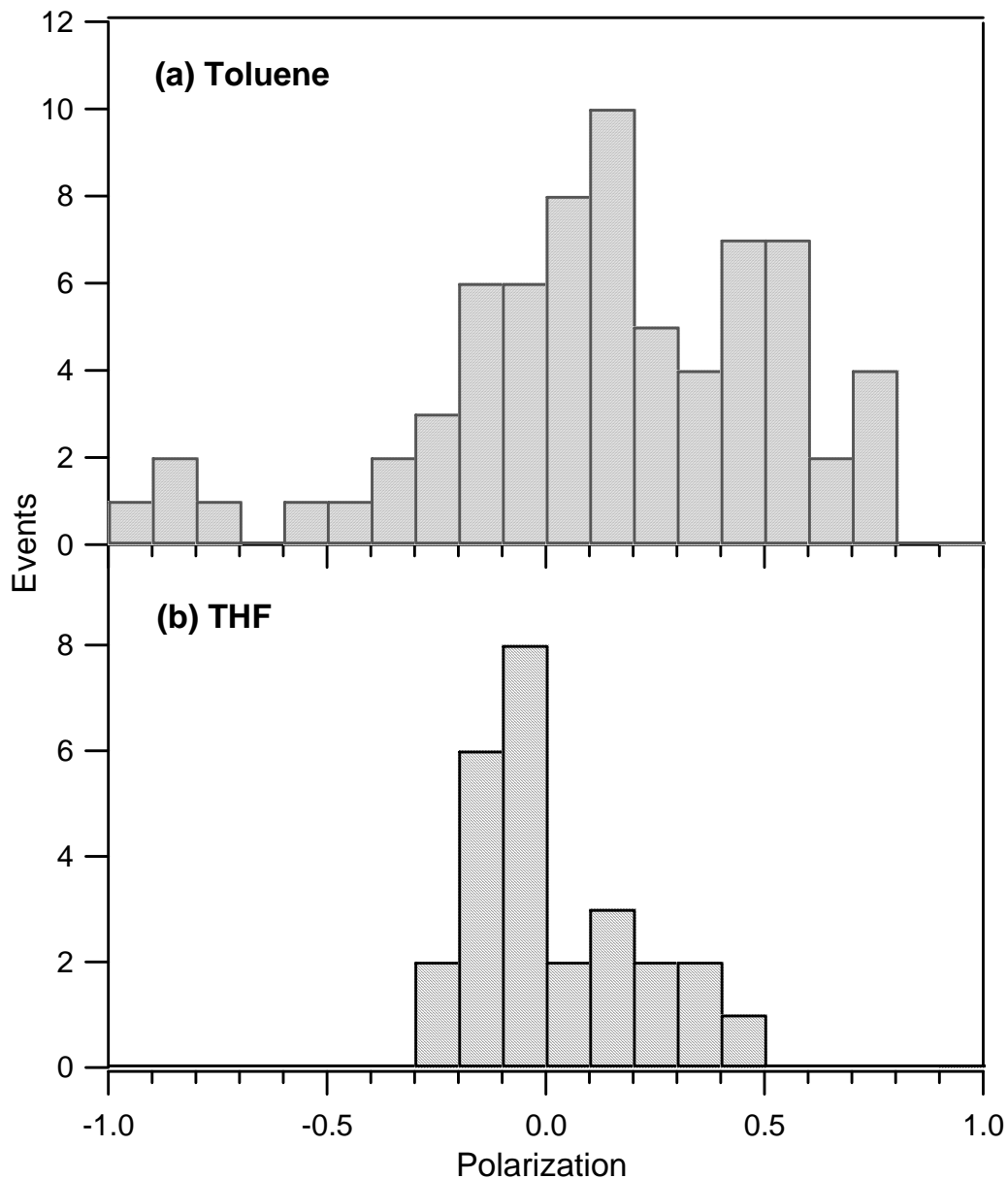
Figure 2.6: Histograms of polarization values of fluorescence, $(I_{//}-I_{\perp})/(I_{//}+I_{\perp})$, of single PFO chains in a PS film cast from the solution using (**a**) toluene or (**b**) THF as a solvent. PFO chains prepared using toluene, have a broader distribution than the other prepared using THF. Average value of (**a**) is 0.124 with a standard deviation value of 0.392, while the average of (**b**) is 0.018 and standard deviation 0.190.

The overall distribution is skewed to polarization parallel to the excitation because of the tendency to study bright molecules which are molecules efficiently excited in the parallel orientation. The distribution of polarization value of molecules cast from THF is markedly different, with most of the molecules show a nearly identical emission in both polarizations leading to a distribution centered at a polarization of zero. The distribution of molecules cast from THF is also slightly skewed towards parallel values because of the linearly polarized excitation. While the orientation of chain or polarizations of emission are not known in the experiment, it is clear that PFO chains are expected to have many emissive sites because it is a multichoromophoric system. If they are coiled and have many emissive sites, linear dichroism values will be close to zero. On the other hand, if the emissive sites on PFO chains are distinct, and the chain has an extended conformation, the value of polarization of emission from PFO has higher chance of being off-zero. According to the distributions of polarization of PFO molecules, it is well evidenced that chain conformation of PFO cast from toluene is more extended than those from THF. Elongated or globular conformation of PFO also can be attributed to the results of different patterns of transients, which will be discussed later in this paper. In the globular conformation of PFO cast from THF, absorbed excitation energy can be easily transferred to many emissive sites leading to isotropic emission and monotonic decays in intensity. On the other hand, elongated conformation of PFO yields energy transfer to particular emissive points and photochemistry leads to large intensity jumps and potentially polarization changes as shown in figure 2.5(a).

34

Emission Spectra of Single Molecules

      While fluorescence transients of total intensity gives information about energy transfer inside molecules, emission spectra collected from fluorescent spots of single PFO in scanned images have advantages of detailed information of changes of blue and green emission band in PFO. Figure 2.7 shows the emission spectrum of a single spot compared to an ensemble spectrum of a pure pristine PFO film collected in a fluorometer. The subtle difference between the spectra is likely the result of small calibration differences between the instruments, rather than a fundamental difference between the single molecule and the ensemble spectrum. High power of laser irradiated onto a PFO causes irreversible photochemical oxidation, i.e. photobleaching inside polymer chain.
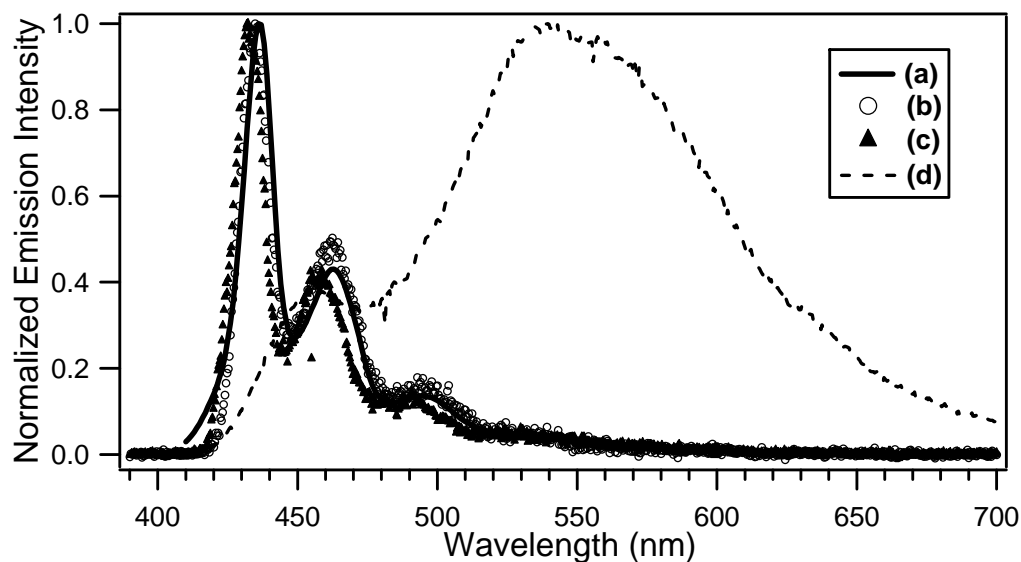
Figure 2.7: Emission spectra of **(a)** a PFO pristine film, **(b)** a single PFO cast from toluene and **(c)** cast from THF and **(d)** pure PFO film after photobleaching. The spectrum of pristine film was taken using commercial UV/VIS spectrometer. Spectra of a single PFO and pure PFO film was taken using the microscope equipped with spectrometer.

By monitoring a series of the fluorescence spectra as a function of time, it is possible to directly probe the changes in the emission that result from photochemistry. Specifically, the appearance of the green emission band associated with fluorenone defects, which is created by photochemical oxidation, can be addressed. Figure 2.8 shows a series of emission spectra from a single molecule collected as a function of time. The spectra decrease in intensity, but otherwise there is no noticeable change in the spectrum. This is universally true for molecules cast from both THF and toluene. This is identical to what has been previously observed for photochemical studies for diluted PFO molecules in a polystyrene matrix.[12] In none of the molecules studied, did the green emission appear upon photobleaching of the molecules. Transients of the intensity in the blue and green regions of the spectrum also indicate no increase in the green emission with photo-oxidation. This implies either that there is no green emission out of defects generated by photobleaching or that the quantum yield from the green emission is so low that the emission is below the detection limit. However, single molecule studies of fluorene/fluorenone copolymers have detected green emission from the fluorenone sites of individual chains.[15] Given this data one would expect that the green emission would be detectable if the photochemistry experiments had produced an emissive fluorenone defect on the polymer chains. The presumed free radical mechanism that leads to fluorenone defects is reported to produce a large number of other photoproducts.[13,34] Bulk studies show extensive crosslinking of the polymer chains can result from oxidation by a prolonged exposure to light, which also produces some fluorenone defects.[13] Based on these previous studies and given that no green emission is detected, the most reasonable account is that few, if any, emissive ketone defects have in fact been generated.
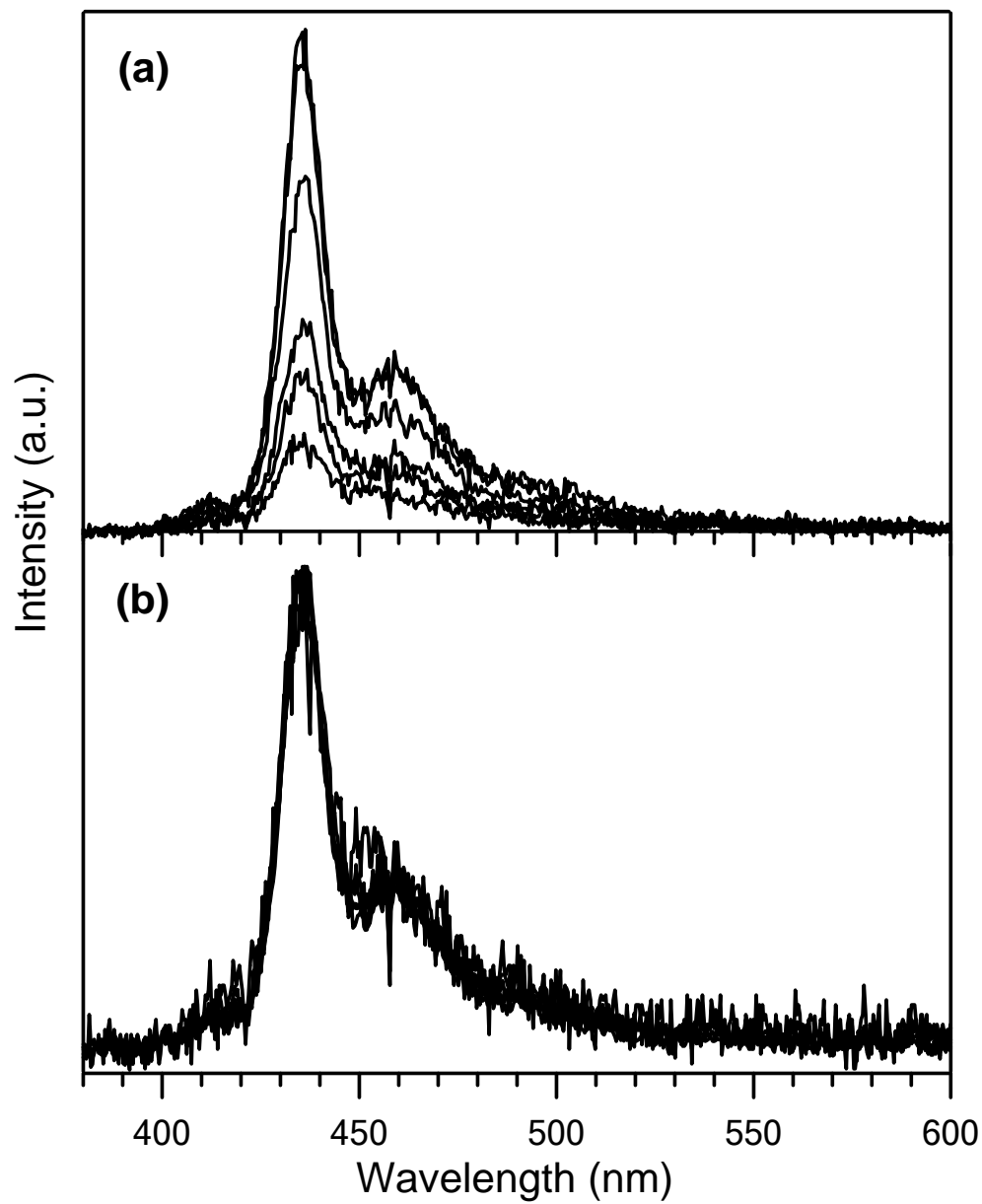
Figure 2.8: A series of emission spectra from a single molecule collected as a function of time during photobleaching process. One is **(a)** unnormalized and the other **(b)** normalized.

Only rarely does photochemical oxidation lead to emissive green defects in the bulk, the defects are prominent as the result of energy transfer.[35] In isolated molecules, they were never observed in our 96 molecules.

Photochemistry of Higher Concentration of PFO Film

While it was reported in another study that fluorenone contributes an enhanced intensity of green emission for PFO single chains,[15] photobleaching of PFO single chains in this study did not lead to a change of structure of the emission spectrum or an appearance of a broad green band. On the other hand, it was observed that emission spectra of pure PFO films showed enhanced green emission after photobleaching as shown in figure 2.7.

Given this data, PS film doped with higher concentration of PFO would be expected to have a greater chance to show an increase in the green emission region, because of the increased population of PFO chains and improved signal to noise ratio. We increased the concentration of PFO in the polystyrene matrix up to about 10 μM which is intermediate concentration between single molecule experiment and pure bulk experiment yet still at a concentration to have isolated chains in PS. Samples were prepared with either toluene or THF as the solvent to compare results with single chain data. Similar to data collection for single PFO chains, repeated measurements of spectra were taken during photochemical oxidation. Examples of spectra are shown in figure 2.9.
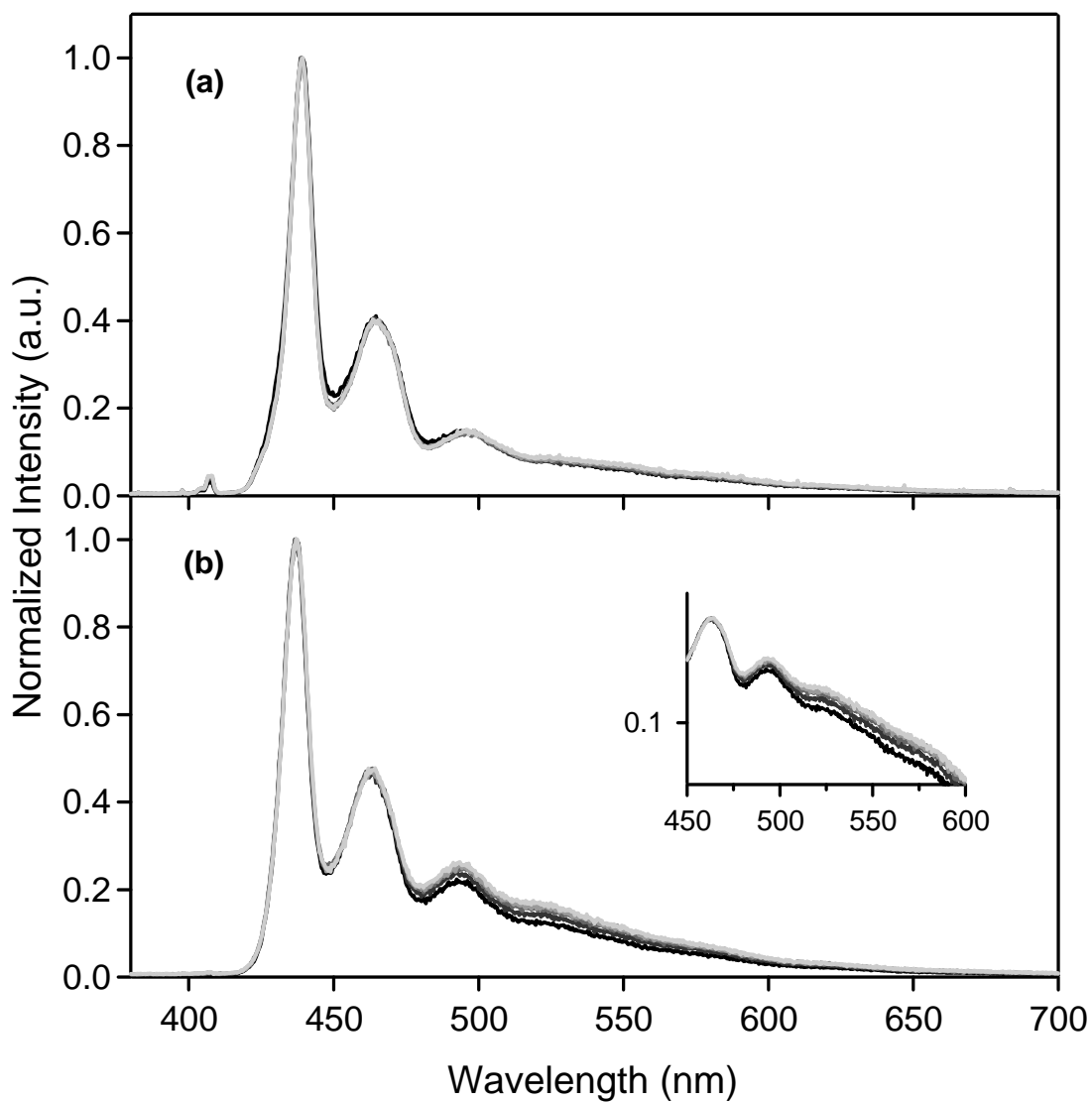
Figure 2.9: A series of emission spectra from a PS film doped with a higher concentration of PFO collected as a function of time during photobleaching process: **(a)** Emission spectra of PFO cast from toluene and **(b)** Emission spectra of PFO cast from THF. The graph of **(b)** in log scale is zoomed in the inset for better comparison. All spectra are normalized to the highest peak. Darker line indicates the spectrum was taken at beginning of the photobleaching and lighter line indicates the spectrum taken later. Time interval between each spectrum is 10 seconds.

Unlike the pure bulk film, in which PFO shows clear degradation of blue emission and a dominance of green emission after photobleaching as shown in figure 2.7, spectra of single chain PFO for both solvent cases didn't lead to spectra dominated by green emission. Each spectrum taken during photobleaching looks similar to the results from single PFO chains. However, close inspection shows slight increase in the green emission in the films cast from THF while the films cast from toluene show almost no change. As shown in figure 2.9, each spectrum from a set of repeated measurements during photobleaching was overlaid after normalization. Spectra from a set of emission spectra collected during photobleaching show a little amount of a broad increase of the peak in the green region after normalization. The darker color of spectrum line, the earlier it was taken. The increase of green emission band in spectra is more outstanding in the case of THF than in the case of toluene. Since the results from polarization measurement in the two different solvents show that the conformation of PFO chains is more globular in THF, we can relate the important role of chain conformation to the degrading blue emission and enhancing green emission. The increase in green in the THF could result in more emissive defects in the globular conformation, greater energy transfer to the defects in this conformation, or necessity for interchain contacts for the green emissive species. The SMS transients show the emission slowly decaying in the THF molecules ruling out extensive energy transfer to single emissive defect sites.

The single molecule studies by Becker *et. al.* would indicate intermolecular interaction are not required for green emission from fluorenone defects. This leaves the formation of more emissive ketone defects in the THF molecules. The greater

intermolecular contacts in THF molecules lead to the formation of more emissive defects than in toluene case.

CONCLUSION

We have investigated emission spectra of ensembles and single chains of PFO doped in PS matrix, and transients of single chains of PFO in PS matrix during photochemical oxidation. The SMS shows the chains cast from THF and toluene have distinct conformations.

The PFO chains are found to be more globular in THF case, while more extended conformation in toluene case. In single molecule experiments, photochemical oxidation of single PFO chain doesn't result in changes of emission spectra and increase in green emission. Total fluorescence intensity decreases during the process and structures of spectra remain same before and after the photobleaching. This indicates that the majority of the photochemistry that results in the loss of fluorescence is not the formation of emissive ketone defect. The ensemble spectra show only very slight increase in green emission in accord with the rare formation of defects. The increase was also dependent on the chain conformation. The SMS never shows green emission as the degradation of the polymer proceeds by many routes rarely producing an emissive defect. On the other hand, ensemble studies of the PFO chains show that molecules cast from THF develop some green emission upon photodegradation while those cast from toluene don't. The increase in green emission in the globular molecules suggests that interchain contacts are necessary for the formation of emissive ketone defects in PFO.

These results also help to understand previously contradictory results in the literature. There are a number of studies showing ketone defects alone are sufficient to produce green emission.[6,11,15,17,22,36] There are also a number of studies that indicate interchain interactions are required.[12-14] All the interchain studies draw their conclusion from the lack of green emission upon oxidation. In the PFO study by Sims, *et al.*,[12] isolated molecules in polystyrene showed identical photobleaching kinetics, but lacked the growth in green emission. In this study the molecules were cast from toluene leading to extended structures. The single molecule studies show that these chains lack green emission upon photo-oxidation, while the copolymer data indicate they should have detectable green component. The lack of emissive defects in the extended chains likely results from the free radical mechanism for the oxidation.[37,38] Polymers with a ketone defects likely have other chemistry occur on neighboring monomers. In the case of the extended chain these monomer are conjugated to the site with the original damage. In the case of the globular chains this damage may involve sites unrelated to the original chromophore.

In summary, not all oxidative damage to the PFO leads to green emission. This does not require that fluorenone excimers are present, but merely that only rare keto defects are emissive. Recent studies have demonstrated that the total green emission does not track with total oxidation.[37] These studies propose regions with multiple fluorenone defects in close proximity lead to enhanced green emission because of the tight packing afforded the polymers without the alkyl sidechains. The globular structure of the THF molecules would afford more close chain contacts that could lead to these emissive defects. Alternatively the chain formation could alter the free radical chemistry generating neighboring defects and/or cross links to the matrix

in extended molecules. While in globular chains chemistry on regions in close proximity may be regions that are at long distances with respect to the extended conjugation. These conclusions could be rigorously tested using non-random copolymers to examine the role of neighboring fluorenone defects and defects in close proximity.

REFERENCES

(1) Shirakawa, H.; Louis, E. J.; MacDiarmid, A. G.; Chiang, C. K.; Heeger, A. J. *J. Chem. Soc., Chem. Commun.* **1977**, 578.

(2) Burroughes, J. H.; Bradley, D. D. C.; Brown, A. R.; Marks, R. N.; Mackay, K.; Friend, R. H.; Burns, P. L.; Holmes, A. B. *Nature* **1990**, *347*, 539.

(3) Gustafsson, G.; Cao, Y.; Treacy, G. M.; Klavetter, F.; Colaneri, N.; Heeger, A. J. *Nature* **1992**, *357*, 477.

(4) Son, S.; Dodabalapur, A.; Lovinger, A. J.; Galvin, M. E. *Science* **1995**, *269*, 376.

(5) Bliznyuk, V. N.; Carter, S. A.; Scott, J. C.; Klaerner, G.; Miller, R. D.; Miller, D. C. *Macromolecules* **1999**, *32*, 361.

(6) Gaal, M.; List, E. J. W.; Scherf, U. *Macromolecules* **2003**, *36*, 4236.

(7) Gamerith, S.; Gadermaier, C.; Scherf, U.; List, E. J. W. *Phys. Status Solidi A* **2004**, *201*, 1132.

(8) Gong, X.; Iyer, P. K.; Moses, D.; Bazan, G. C.; Heeger, A. J.; Xiao, S. S. *Adv. Funct. Mater.* **2003**, *13*, 325.

(9) Montilla, F.; Mallavia, R. *Adv. Funct. Mater.* **2007**, *17*, 71.

(10) Pogantsch, A.; Zaami, N.; Slugovc, C. *Chem. Phys.* **2006**, *322*, 399.

(11) Romaner, L.; Pogantsch, A.; Scandiucci de Freitas, P.; Scherf, U.; Gaal, M.; Zojer, E.; List, E. J. W. *Adv. Funct. Mater.* **2003**, *13*, 597.

(12) Sims, M.; Bradley, D. D. C.; Ariu, M.; Koeberg, M.; Asimakis, A.; Grell, M.; Lidzey, D. G. *Adv. Funct. Mater.* **2004**, *14*, 765.

(13) Zhao, W.; Cao, T.; White, J. M. *Adv. Funct. Mater.* **2004**, *14*, 783.

(14) Aharon, E.; Albo, A.; Kalina, M.; Frey, G. L. *Adv. Funct. Mater.* **2006**, *16*, 980.

(15) Becker, K.; Lupton, J. M.; Feldmann, J.; Nehls, B. S.; Galbrecht, F.; Gao, D.; Scherf, U. *Adv. Funct. Mater.* **2006**, *16*, 364.

(16) Dias, F. B.; Maiti, M.; Hintschich, S., I.; Monkman, A. P. *J. Chem. Phys.* **2005**, *122*, 54904.

(17) Hintschich, S. I.; Rothe, C.; Sinha, S.; Monkman, A. P.; Scandiucci de Freitas, P.; Scherf, U. *J. Chem. Phys.* **2003**, *119*, 12017.

(18)   List, E. J. W.; Gaal, M.; Guentner, R.; Scandiucci de Freitas, P.; Scherf, U. *Synth. Met.* **2003**, *139*, 759.

(19)   Romaner, L.; Piok, T.; Gadermaier, C.; Guentner, R.; Scandiucci de Freitas, P.; Scherf, U.; Cerullo, G.; Lanzani, G.; List, E. J. W. *Synth. Met.* **2003**, *139*, 851.

(20)   Zhou, X.-H.; Zhang, Y.; Xie, Y.-Q.; Cao, Y.; Pei, J. *Macromolecules* **2006**, *39*, 3830.

(21)   Dias, F. B.; Knaapila, M.; Monkman, A. P.; Burrows, H. D. *Macromolecules* **2006**, *39*, 1598.

(22)   Zhou, J.-J.; Li, J.; Fu, Y.-Q.; Bo, Z.-S.; Li, L.; Chan, C.-M. *Polymer* **2007**, *48*, 2503.

(23)   Barbara, P. F.; Gesquiere, A. J.; Park, S.-J.; Lee, Y. J. *Acc. Chem. Res.* **2005**, *38*, 602.

(24)   Grey, J. K.; Kim, D. Y.; Lee, Y. J.; Gutierrez, J. J.; Luong, N.; Ferraris, J. P.; Barbara, P. F. *Angew. Chem., Int. Ed. Engl.* **2005**, *44*, 6207.

(25)   Huser, T.; Yan, M.; Rothberg, L. J. *Proc. Natl. Acad. Sci. U. S. A.* **2000**, *97*, 11187.

(26)   Kim, D. Y.; Grey, J. K.; Barbara, P. F. *Synth. Met.* **2006**, *156*, 336.

(27)   Hu, D.; Yu, J.; Barbara, P. F. *J. Am. Chem. Soc.* **1999**, *121*, 6936.

(28)   Vanden Bout, D. A.; Yip, W.-T.; Hu, D.; Fu, D.-K.; Swager, T. M.; Barbara, P. F. *Science* **1997**, *277*, 1074.

(29)   Yip, W.-T.; Hu, D.; Yu, J.; Vanden Bout, D. A.; Barbara, P. F. *J. Phys. Chem. A* **1998**, *102*, 7564.

(30)   Surin, M.; Hennebicq, E.; Ego, C.; Marsitzky, D.; Grimsdale, A. C.; Müllen, K.; Brédas, J.-L.; Lazzaroni, R.; Leclère, P. *Chem. Mater.* **2004**, *16*, 994.

(31)   Nguyen, T.-Q.; Doan, V.; Schwartz, B. J. *J. Chem. Phys.* **1999**, *110*, 4068.

(32)   Hu, D.; Yu, J.; Wong, K.; Bagchl, B.; Rossky, P. J.; Barbara, P. F. *Nature* **2000**, *405*, 1030.

(33)   Sun, W.-Y.; Yang, S.-C.; White, J. D.; Hsu, J.-H.; Pern, G. Y.; Chen, S. A.; Fann, W. *Macromolecules* **2005**, *38*, 2966.

(34)   Liu, L.; Tang, S.; Liu, M.; Xie, Z.; Zhang, W.; Lu, P.; Hanif, M.; Ma, Y. *J. Phys. Chem. B* **2006**, *110*, 13734.

(35)   Rozanski, L.; Cone, C.; Ostrowski, D.; Vanden Bout, D. A. *Macromolecules* **2007**, *40*, 4524.

(36)   Chochos, C. L.; Kallitsis, J. K.; Gregoriou, V. G. *J. Phys. Chem. B* **2005**, *109*, 8755.

(37)   Grisorio, R.; Suranna, G. P.; Mastrorilli, P.; Nobile, C. F. *Adv. Funct. Mater.* **2007**, *17*, 538.

(38)   Liu, L.; Qiu, S.; Wang, B.; Zhang, W.; Lu, P.; Xie, Z.; Hanif, M.; Ma, Y.; Shen, J. *J. Phys. Chem. B* **2005**, *109*, 23366.

Chapter 3: Photochemistry of Aggregated and Non-aggregated Polyfluorene: the Franck-Condon Progression Model Analysis

INTRODUCTION

The properties of conjugate polymers have been of great interest to many research groups for a decade since their introduction, mainly because of potential applications in photovoltaic devices such as organic light-emitting diodes (OLEDs), solid state lasers and thin-film transistors.[1] Polyfluorene is a conjugate polymers that have, recently, started to get attention because of its promising performance in developing electronic devices.[2] It also has attracted attention as a good material for blue emission with its sharp intense emission near 430 nm, high photoluminescence yield, and high hole mobility, despite its limitation of degeneration of blue emission to green[2]. Furthermore, the liquid crystalline behavior of polyfluorene opens possibility of making a polarized light emitting polymer films.[3] It is well known that optical property of PFO thin films are affected by film morphology and photochemistry occurring along the polymer chain.[4-7] The optical and electronic properties of polyfluorene have been widely discussed and great understanding has been brought to us by many research groups. However, the limitation still lies in understanding photochemistry of polyfluorene during photooxidation associated with the appearance of green emission band in its emission spectrum.

Complicated coupling of electronic properties to structural changes is of special importance in the case of conjugate polymers. The Huang-Rhys parameter, S,

is the parameter that makes optical properties sensitive to conformational and thermal disorder by modifying the vibronic structures in the electronic spectra[8,9]. In conjugate polymer, the delocalization length of π electron is affected by structural disorder of the polymer backbone[10]. A smaller Huang-Rhys parameter is attributed to the increase in the effective conjugation length, because structural deformation of excited states in π conjugated polymer is reduced with increasing conjugation length, which leads to less electron-phonon interaction with less probability of sub-zero phonon transition line[10]. The Huang-Rhys parameter, thus, exhibits the close relations between the S-parameter and conjugation length of the polymer. These characteristics of Huang-Rhys parameter give an easy and instant way to study the electronic changes and photochemistry of the polymer during a process. When Franck-condon principle governs the process of emission in the system, the Franck-Condon progression model can describes well the shape of emission spectra given by

$$I_{ba}(E) = I_0 \sum_n \frac{e^{-S} S^n}{n!} \delta(E_0 - n\hbar\omega - E),$$
(Eq. 3.1)

where E_0 is the energy of zero-phonon transition, S the Huang-Rhys parameter, I_0 the intensity of full emission band, ω angular frequency, and n the number of vibrational overtones. S is a rough measure of the number of vibrations generated during the relaxation of excited molecules to the new configuration in the excited states. According to the equation above, the zero-phonon line has the intensity of $I_0 e^{-S}$, and if $S=0$, the total intensity is equal to the intensity of the zero-phonon line. As S increases, the intensity of zero-phonon line decreases and it is compensated for by

the appearance of vibrational side bands. Sub-zero phonon line is expressed by the equation below:

$$I_{0\to n} \propto \frac{e^{-S}S^n}{n!} \qquad \text{(Eq. 3.2)}$$

Therefore, the value of S can be calculated from

$$\frac{I_{0\to 1}}{I_{0\to 0}} = S \qquad \text{(Eq. 3.3)}$$

In this work, photochemistry of polyfluorene during photooxidation is investigated using Huang-Rhys parameter analysis. The effects of chain morphology of polyfluorene, aggregated or non-aggregated, is discussed with respect to S-parameter.

EXPERIMENTAL SECTION

Commercial poly(9,9-dioctylfluorenyl-2,7-diyl) (PFO, American Dye Source, Inc., ADS129BE) was used without further purification. Molecular weight of PFO ranged from 40 kDa ~ 120 kDa. Polystyrene (PS) was purchased from Aldrich and used without additional purification. PFO solution and polystyrene solution were prepared with tetrahydrofuran (THF). Concentration was maintained at about 1wt%. Thin films of PFO were prepared with a spin coater (Specialty Coating Systems Inc., Model P6204-A). PFO in PS solution was spun-cast onto a glass coverslip rotating at

about 2000 rpm for 20 seconds. The film of non-aggregated PFO was prepared by applying mild heat until the solution changed from yellow to colorless. All samples were placed in vacuum seal container to evaporate solvent remaining in samples.

The samples at room temperature were excited using a 405 nm CW laser (Coherent Auburn Division, Blue/violet Diode Laser System) by illuminating the sample off a dichroic mirror and through a 1.25 numerical aperture microscope objective in an epi configuration. The polarization of excitation beam was linear such that it was s-polarized with respect to the dichroic mirror. Laser power was attenuated to about 1.5 μW to control the decay rate of total fluorescence during photooxidation process. The fluorescence was collected through the same microscope objective and imaged onto a spectrometer (Acton) equipped with a CCD camera (Princeton Instruments, LN-400EB).

DATA ANALYSIS

Fluorescence from thin film of PFO is collected every 10 second and exposure time for each collection is 10 seconds. One set of examples of emission spectra of aggregated and non-aggregated PFO film is shown in figure 3.1. The total fluorescence intensity decreases as the photooxidation proceeds, because the high power of excitation. The noticeable difference between the emission spectra of aggregated PFO and non-aggregated PFO is observed in the intensities of 0-1 peak after normalizing spectra to the intensity of 0-0 phonon line.
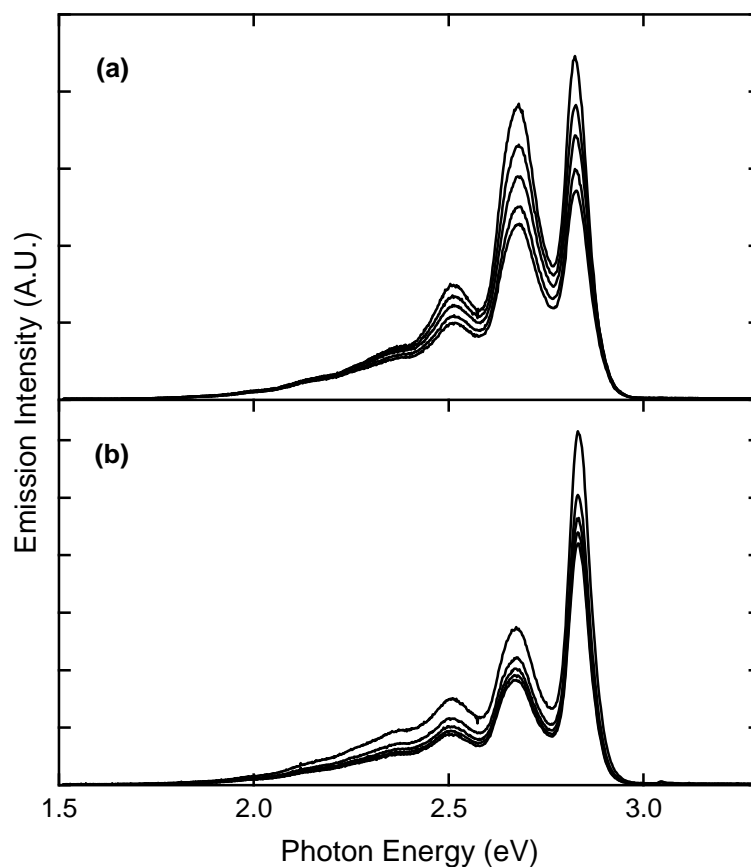
Figure 3.1: The time-resolved emission spectra of **(a)** aggregated PFO and **(b)** non-aggregated PFO collected during photooxidation are plotted together for illustrating the change of intensity and spectral structures. Time interval between each spectrum is 20 seconds. Note the intensity difference of 0-1 transition phonon line between two spectra.

The intensity of 0-1 peak in the aggregated PFO film is larger than that in the non-aggregated ones. The effort to explain the difference in the emission spectra depending on film condition is carried out by fitting them to the Franck-Condon progression model using the (Eq. 3.1). All spectra of a set of collection are normalized to the intensity of 0-0 transition peak and fitted using the (Eq. 3.1) for analysis.

Figure 3.2: The fitting results of emission spectra of **(a)** aggregated and **(b)** non-aggregated PFO using the (Eq. 3.1).

One of the fitting results is exemplified in figure 3.2. For simplification, each peak is represented by a simple Gaussian function with same widths. As the results of the vibronic progression occurring in the excited PFO films,[10] both the spectra and fitting function display gradual decrease in their peaks as the energy of the peaks decreased. However, the broader widths of peaks at lower energy, which is believed to come from disorder of the PFO films, produce significant errors in fitting overall. This problem can be overcome by the introduction of an increase of the width of peaks for higher vibronic peaks. This improves the results dramatically with the assumption

52

that the width of peaks becomes larger as the energy of the peaks decrease. To systematically include this assumption into the Frank-Condon progression model, the (Eq. 3.1) is modified into the following:

$$I_{ba}(E) = \sum_n \frac{e^{-S}S^n}{n!} I_0(\sigma_0 + n\sigma_1) \cdot \delta(E_0 - n\hbar\omega - E),$$

(Eq. 3.4)

where the width of peaks increase by the increment of σ_1 starting from σ_0. All spectra are fitted to the modified Franck-Condon progression using the (Eq. 3.4). The modified Franck-Condon progression model displayed improved fitting results at higher energy region, as shown in figure 3.3(a) and (b). But, the problem still exists so that the (Eq. 3.4) cannot account for the lower energy region resulting in significant errors. The difference in the lower energy between the model and the experimental data suggests a key that another component other than the Franck-Condon progression components needs to explain the discrepancy. In figure 3.3(c), the differences between the experimental spectrum and the fitting results by the (Eq. 3.4) are plotted together with a scaled experimental green-peaked emission spectrum of photooxidized PFO film. It is notable that they all exhibit qualitative resemblance excluding the fitting error in the higher energy. As it is well known that defects along the PFO polymer chain cause an increase of green emission in its photoluminescence spectra,[2,4,6,7,11-15] it is reasonable to add one additional independent component into the Franck-Condon progression model to account for the structure of the emission spectra in both the aggregated and the non-aggregated PFO.
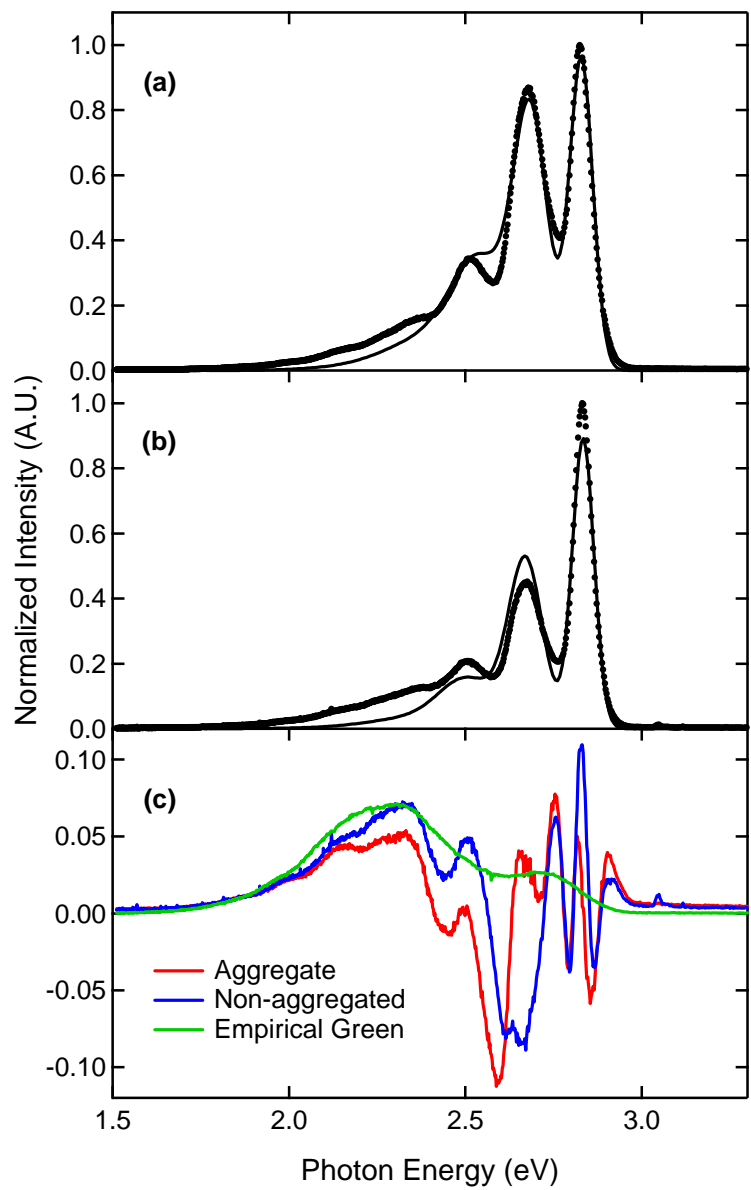
Figure 3.3: The fitting results of emission spectra of **(a)** aggregated PFO and **(b)** non-aggregated PFO using Eq.(4) and **(c)** the difference between experimental emission spectra and the fitting results by using Eq. (4). The green-peaked emission spectrum of photooxidized PFO is scaled and plotted together for comparison.

In accordance with the result, the Franck-Condon progression model is modified again for fitting by introducing an additional independent Gaussian component, I_A. The best Gaussian fit of the empirical the green-peaked emission spectrum of PFO (Figure 3.4) is used for I_A, making the fitting equation below:

$$I_{ba}(E) = \sum_n \frac{e^{-S}S^n}{n!} I_0(\sigma_0 + n\sigma_1) \cdot \delta(E_0 - n\hbar\omega - E) + I_A. \qquad \text{(Eq. 3.5)}$$
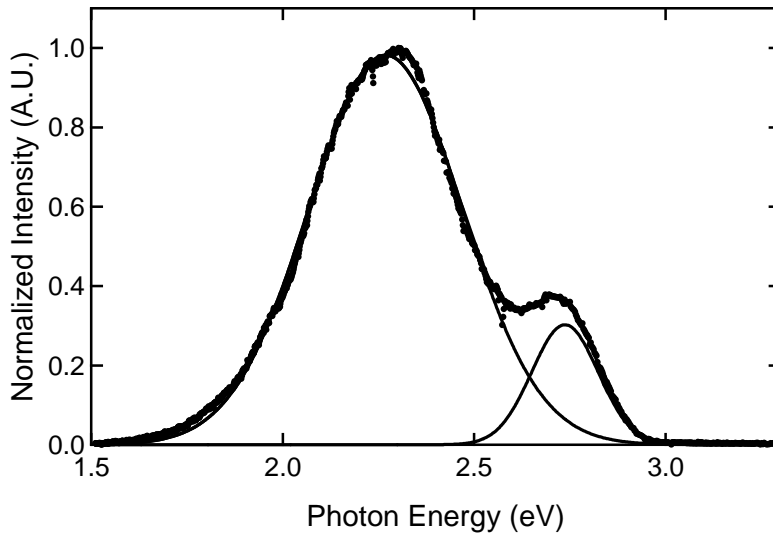
Figure 3.4: The fitting results (—) of green-peaked emission spectrum (●) of photooxidized PFO films using two independent Gaussina functions. The resultant fitting parameters of left Gaussian function are 0.9821 for amplitude, 2.2691 for peak center, and 0.20056 for width at FWHM; those of right Gaussian functions 0.30225 for amplitude, 2.7371 for peak center, and 0.086965 for width at FWHM.

The empirical green-peaked spectrum of photo-oxidized pure PFO film using 405 nm is used for the purpose. The empirical green-peaked spectrum of PFO falls into a good fit by using two independents Gaussian functions. However, the smaller peak at the higher energy is excluded in fitting, because it is possibly a residual peak from the

55

spectrum of before-oxidized PFO. It is confirmed that the effect of the excluded Gaussian function of the empirical spectrum fitting is minimal and restricted to the its energy range, not the whole results of fitting. An example of fitting suing (Eq. 3.5) is shown in figure 3.5. The modified Franck-Condon progression model with empirical green component of PFO works better in fitting emission spectra of PFO. This suggests that the emission spectra of PFO consist of two photochemical species.
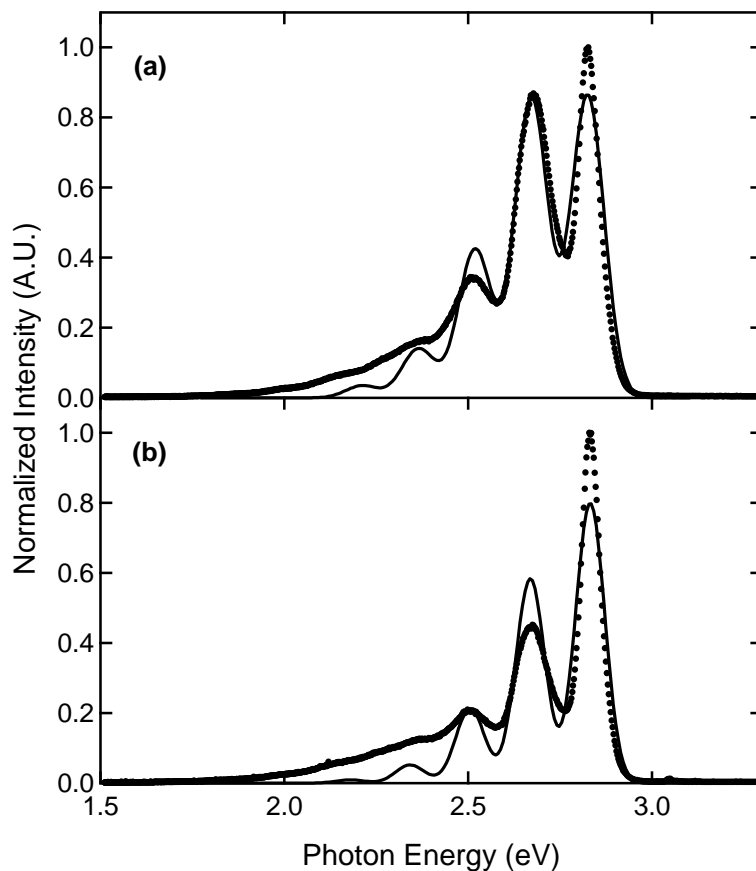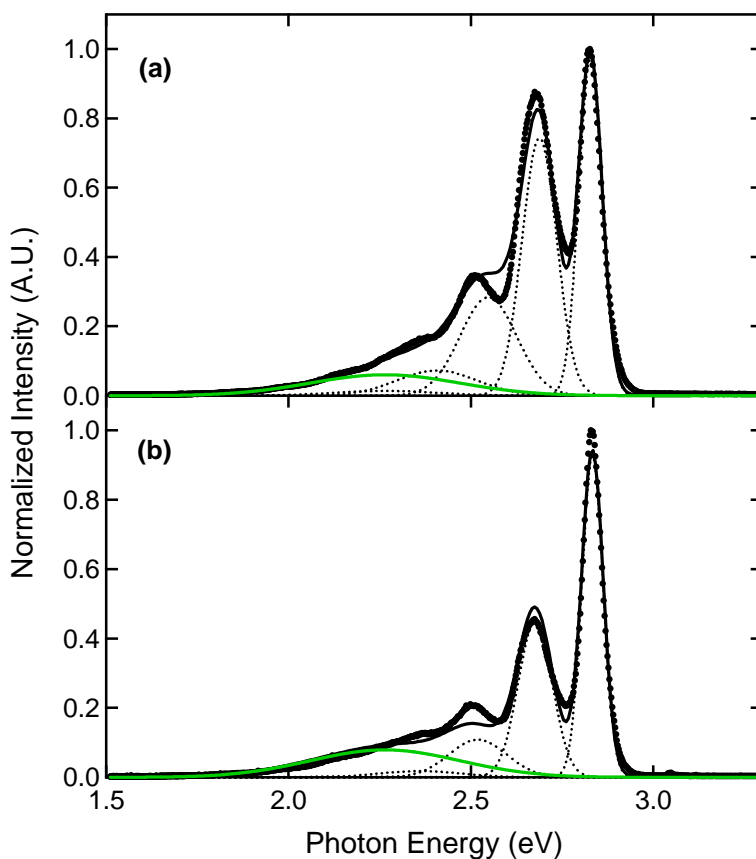

Figure 3.5: The fitting results (—) of emission spectra (●) of **(a)** aggregated and **(b)** non-aggregated PFO using Eq. (5). Dashed lines represent each Gaussian replica from modified Franck-Condon progression model. Green solid line is a empirical green-peaked emission spectra of PFO, which is scaled for the best fit.

56

RESULTS AND DISCUSSIONS

In accordance with Franck-Condon principles for emission $S_1{\rightarrow}S_0$ 0-n, each fitted Gaussian peak can be assigned to 0-0, 0-1, 0-2 transition, etc. in the fitting results[10]. The positions of all peaks remain same because $\hbar\omega$ remains almost constant during photooxidation and conditions of the PFO don't make noticeable difference. The averages of $\hbar\omega$ of aggregated and non-aggregated PFO are $0.1467{\pm}0.0002$ eV and $0.1587{\pm}0.0002$ eV, respectively. The values are close to the 0.18 eV of C=C symmetric stretching of polyfluorene backbone, which is expected to dominate the coupling to electronic transition. It is noted that the values are also close to those of in-plane C-H bending, which are abundant in substituted alkyl group of PFO backbone. It accounts for the difference of frequency of the C=C stretching mode of the polymer backbone. The widths of the Gaussians in Franck-Condon components also don't show much change during the photooxidation. The widths of 0-0 peaks of aggregated and non-aggregated PFO are $0.0352{\pm}0.0003$ eV and $0.0301{\pm}0.0002$, and the widths of 0-1 peaks $0.0665{\pm}0.0003$ eV and $0.0687{\pm}0.0002$ eV, respectively. In the meantime, the Huang-Rhys parameter, *S*, which has an implication of the conjugation length of conjugate polymer, also displays negligible increases both in aggregated and non-aggregated PFO (Figure 3.6).The averages of *S* of aggregated and non-aggregated PFO films are $0.737{\pm}0.008$ and $0.501{\pm}0.002$, respectively. In the modified Franck-condon progression model, Gaussians are related to vibrational mode of the polymer molecule in accordance with the Franck-Condon principle by means of Huang-Rhys parameter. In the analysis of emission spectra of conjugate

polymer, the dimensionless Huang-Rhys parameter corresponds to the average number of phonons involved during relaxation and has directly something to do with the effective conjugation of polymers. The smaller value of S means the more enhanced conjugation of polymers, which results in less probability of sub-zero phonon lines in their emission spectra. As the modified Franck-Condon model is a good fit to emission spectra of PFO, the Huang-Rhys parameters, S, are estimated from the fitting results of emission spectra using Eq. (5). As the all portions of emission spectra of PFO don't exactly follows the Franck-Condon principle because of other factors, such as other photochemical species, photooxidation, and so on, the Huang-Rhys parameter, S, doesn't necessarily have correspondence to the conjugation length of conjugate polymer. However, as the modified Franck-Condon progression model works fairly in blue emission region, it still provides qualitative pictures of conjugation length. The parameters for the aggregated PFO are larger than that for the non- aggregated PFO during whole photooxidation, which may imply that the conjugation length of aggregated PFO is shorter than that of non-aggregated PFO. Because of the heat applied to prepare non-aggregated PFO film, the conjugation length of PFO is believed to become longer in non-aggregated PFO films than in aggregated PFO films. As the photochemistry in the design of study doesn't change chain morphology in films but cause many irreversible photochemical processes in polymer itself, the decrease of S of non-aggregated PFO hardly means the change of conjugation length of polymer. However, it is possible that the very small decrease of conjugation in PFO films occurs upon photooxidation. It can be supported by the very small increase of the S parameters both in aggregated and in non-aggregated PFO.
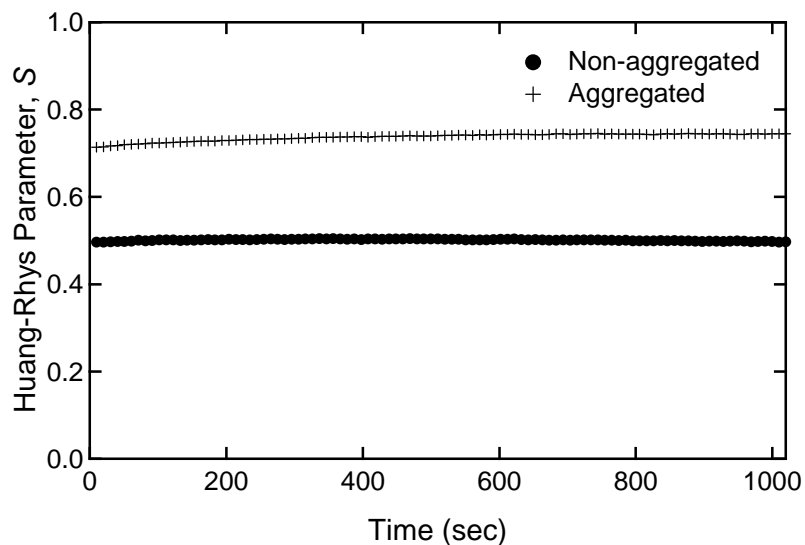
Figure 3.6: The change of Huang-Rhys parameter, *S*, over photooxidation time.
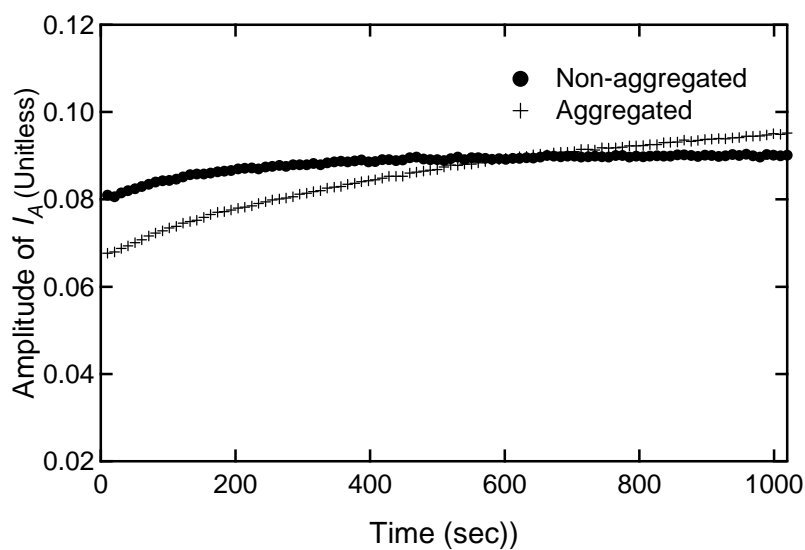
Figure 3.7: The change of the amplitude of empirical green-peaked emission
spectrum of PFO.

In the meantime, the amplitude of the empirical independent Gaussian function exhibits monotonic increases during the photooxidation and the change in aggregated PFO case is more noticeable than that in non-aggregated PFO (Figure 3.7). The photooxidation is a destructive process in which the total fluorescence is decreased as it proceeds as shown in figure 3.1. Upon being excited by a high power of laser, PFO undergoes many processes such as 0-0 transition, 0-1 transition, and destruction of chromophore competing one another. As discussed earlier in this section, presumably, the independent Gaussian corresponds to different photochemistry process than other Gaussians from Franck-Condon model, i.e. green emission by oxidation. It can also be evidenced by the fitting results of emission spectrum of single PFO molecule. In the previous study, the single PFO chains didn't yield measurable increase of green emission, when it was photochemically oxidized.[16] When the fitting of emission spectrum of single PFO chain is done using the modified Franck-Condon progression model, (Eq. 3.4) *without* empirical green-peaked term included, as shown in figure 3.8, there is not significant error found in the lower energy region. Therefore, it is interesting to monitor the values and changes of the amplitude of the independent Gaussian peak not from the Franck-Condon model. The amplitude of the independent green component Gaussian increases both at the aggregated and the non-aggregated PFO, which implies that more green emission accounts for the total emission from PFO as the photooxidation proceeds. As the all spectra are normalized, the absolute values of the amplitude are of a little significance. However, the plot of aggregated PFO is steeper and the value becomes bigger than those of non-aggregated PFO. As studied in previous study, chain morphology plays role when all ketone defects generated by photooxidation are not

60

efficiently emissive.[16] Probably, it suggests that the more interchain interaction in the aggregated PFO than non-aggregated PFO, the more green emission generated in PFO. It shows same results as in many previous works[6,7,11] claiming that interchain interaction has closely something to do with the appearance of green emission of PFO.
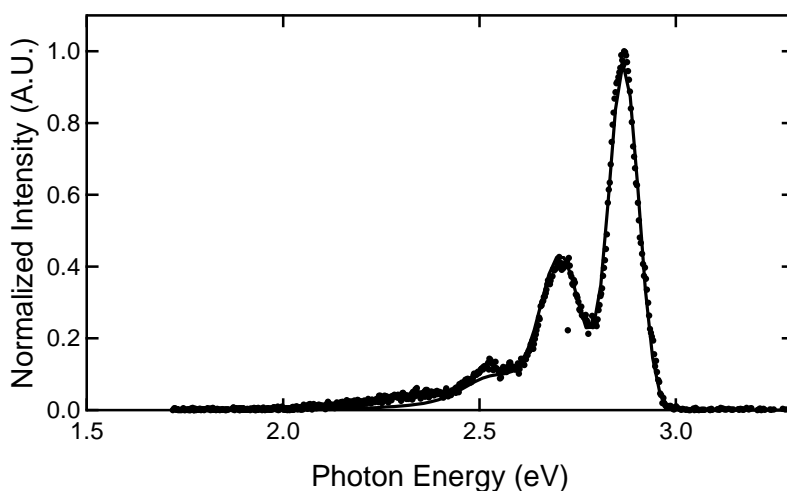
Figure 3.8: The fitting result (—) of emission spectrum of PFO single molecule(●). The modified Franck-Condon progression model using the Eq. (4) is used here. The resultant Huang-Rhys parameter is 0.435±0.004.

CONCLUSION

The photochemistry of aggregated or non-aggregated poly(9,9-dioctylfluorenyl-2,7-diyl) during photooxidation is investigated. All emission spectra are analyzed by fitting them to modified Franck-Condon progression model including empirical green-peaked emission spectrum of PFO. It provides information about

photochemistry of photooxidation of PFO films with a focus on the change of green emission in the meantime. A spectrum of thin film of PFO displayed stronger intensity in 0-1 transition peak when the polymer is aggregated than when is not aggregated. The Huang-Rhys parameter, S, with implication of conjugation length of polymer exhibited very negligible increase in both conditions, demonstrating longer conjugation length of the polymer becomes short. The parameter also turned out smaller values in non-aggregated PFO film, which means the conjugation length is longer in non-aggregated PFO film because of the heat applied to prepare non-aggregated PFO. The photooxidation doesn't have an effect to change the morphology of polymer Therefore, the very small changes of S both in non-aggregated and aggregated PFO are believed to come from destructive process of fluorescence by continuous excitation with high power. In the mean time, the amplitude of empirical green-peaked emission of both aggregated and non-aggregated PFO increased, implying that the green emission of PFO increased relatively as a result of photooxidation. The slope of the increase was steeper in aggregated PFO than in non-aggregated PFO. As there is more interchain interaction in aggregated PFO film, the larger amount of green emission in aggregated PFO comes from the existence of more chances of interchain interaction and this is in a good agreement with the results of many previous works. It is well supported by the fact that the analysis of emission spectra of single PFO chain turned out to be in good match to Franck-Condon progression model without introducing any additional components

In conclusion, the emission of aggregated PFO films contains more portion of green emission than non-aggregated PFO films. The more interchain interaction is responsible for the improved green emission upon photooxidation as discussed in

many previous works. The emission of PFO consists of two photochemical species which follow either Franck-Condon model or non-Franck-Condon model. Franck-Condon model mainly accounts for the sharp intensity of blue and its progression in the spectrum, while the non-Franck-Condon model explains the improved green emission of photo-oxidized PFO.

REFERENCES

(1) Friend, R. H.; Gymer, R. W.; Holmes, A. B.; Burroughes, J. H.; Marks, R. N.; Taliani, C.; Bradley, D. D. C.; Dos Santos, D. A.; Bredas, J. L.; Logdlund, M.; Salaneck, W. R. *Nature* **1999**, *397*, 121.

(2) Bliznyuk, V. N.; Carter, S. A.; Scott, J. C.; Klaerner, G.; Miller, R. D.; Miller, D. C. *Macromolecules* **1999**, *32*, 361.

(3) Whitehead, K. S.; Grell, M.; Bradley, D. D. C.; Jandke, M.; Strohriegl, P. *Appl. Phys. Lett.* **2000**, *76*, 2946.

(4) Becker, K.; Lupton, J. M.; Feldmann, J.; Nehls, B. S.; Galbrecht, F.; Gao, D.; Scherf, U. *Adv. Funct. Mater.* **2006**, *16*, 364.

(5) Dias, F. B.; Maiti, M.; Hintschich, S., I.; Monkman, A. P. *J. Chem. Phys.* **2005**, *122*, 54904.

(6) Sims, M.; Bradley, D. D. C.; Ariu, M.; Koeberg, M.; Asimakis, A.; Grell, M.; Lidzey, D. G. *Adv. Funct. Mater.* **2004**, *14*, 765.

(7) Zhao, W.; Cao, T.; White, J. M. *Adv. Funct. Mater.* **2004**, *14*, 783.

(8) Henderson, B.; Imbusch, G. F. *Optical spectroscopy of inorganic solids*; Oxford University Press: New York, 1989.

(9) Huang, K.; Rhys, A. *Proc. R. Soc. London, A* **1950**, *204*, 406.

(10) Bässler, H.; Schweitzer, B. *Acc. Chem. Res.* **1999**, *32*, 173.

(11) Aharon, E.; Albo, A.; Kalina, M.; Frey, G. L. *Adv. Funct. Mater.* **2006**, *16*, 980.

(12) Gaal, M.; List, E. J. W.; Scherf, U. Macromolecules **2003**, *36*, 4236.

(13) Gamerith, S.; Gadermaier, C.; Scherf, U.; List, E. J. W. *Phys. Status Solidi A* **2004**, *201*, 1132.

(14) Gong, X.; Iyer, P. K.; Moses, D.; Bazan, G. C.; Heeger, A. J.; Xiao, S. S. *Adv. Funct. Mater.* **2003**, *13*, 325.

(15) Montilla, F.; Mallavia, R. *Adv. Funct. Mater.* **2007**, *17*, 71.

(16) Kim, Y. H.; Vanden Bout, D. A. *J. Phys. Chem. B*, *in preparation*.

Chapter 4:   Single Molecule Studies of Non-exponentiality of Rotation Dynamics of Rhodamine6G in Poly(methyl acrylate) matrix

INTRODUCTION

Instead of being crystallized at a melting point, T_m, amorphous materials become a so-called supercooled liquid material (Figure 1.3).[1-5] Upon continuous cooling down, the property of the amorphous material shows singularity in its cooling curve and has too little mobility below the singular point to show "slowing down" dynamics[6,7] which cannot be measured within a reasonable experimental time window. The nature of an amorphous material such as polymers, viscous liquid, etc. near glass transition temperature has been of interest for decades.[1-17] Most notably, the exponential decay form of the relaxation process in liquid phase changes their characters to become a highly non-exponential decay near glass transition temperature. The single exponential decay of property of normal liquid at room temperature clearly have been investigated by the approach of a Brownian diffusional process model,[18,19] while non-exponential decay of supercooled liquid near glass transition temperature has needed complicated method to probe. Therefore, it is the supercooled material of which dynamics have been of interest in previous studies for decades.[1-17] As a class of one of the representative materials among amorphous material, the dynamics of glass forming polymer[1-5,20] has interested many research groups as well. One of the most popular materials under study is poly(methyl

acrylate) (PMA) of which glass transition temperature is reportedly estimated 276~291 K in calculation and experiment.[14,21-23] In the previous works of bulk measurements, non-exponential behavior of rotational dynamics of a supercooled polymer near glass transition temperature was reported in other previous studies.[13,16,20] Another interesting nature of dynamics of materials in supercooled liquid lies in their heterogeneity,[1-5,10-12,15,17,24-27] which is originally involved in the first theoretical approach to the dynamics of supercooled liquid.[3,8] The result of non-exponential decay of dynamics relaxation in bulk measurement could come from two possibilities[1,2,10,12,17]: (1) the time constant of dynamics of sub-ensemble varies substantially but, each dynamical relaxation is intrinsically in the form of single exponential decay. In result, the ensemble measurement is non-exponential and the dynamics of sub-ensemble is "heterogeneous". Or, (2) the time constants of dynamics of sub-ensembles are perceived inherently to be non-exponential but all same one another, which has an outcome of non-exponential decay of ensemble in consequence. In this case, the "homogeneous" scenario goes into work. It is necessary to probe small subdomain of sample to have conclusion reach to either one of them.

To expedite the non-exponentiality of rotational dynamics of Rhodamine 6G embedded in PMA and its heterogeneity, the results from single molecule spectroscopic techniques[28-32] are presented in this chapter. It provides possibility of better understanding the characteristics and the origin of macroscopic non-exponentiality[1-4] of rotational dynamics of PMA near glass transition temperature.

EXPERIMENTAL SECTION

Sample Preparation and Experimental Setup

Poly(methyl acrylate) (PMA), of which chemical structure is shown in figure 4.1(a), was purchased from Aldrich and used without further purification. Rhodamine 6G (R6G) was purchased from Spectra-Physics and used as a probe molecule. Toluene was used to prepare 1 wt% PMA solution and R6G stock solution. Dye solution was diluted up to 0.1 nM using PMA solution so that single dye molecules can be well separated in PMA thin film. Thin films were prepared with a spin coater (Specialty Coating Systems Inc., Model P6204-A) at 2000 rpm for 20 seconds.

(a)

(b)
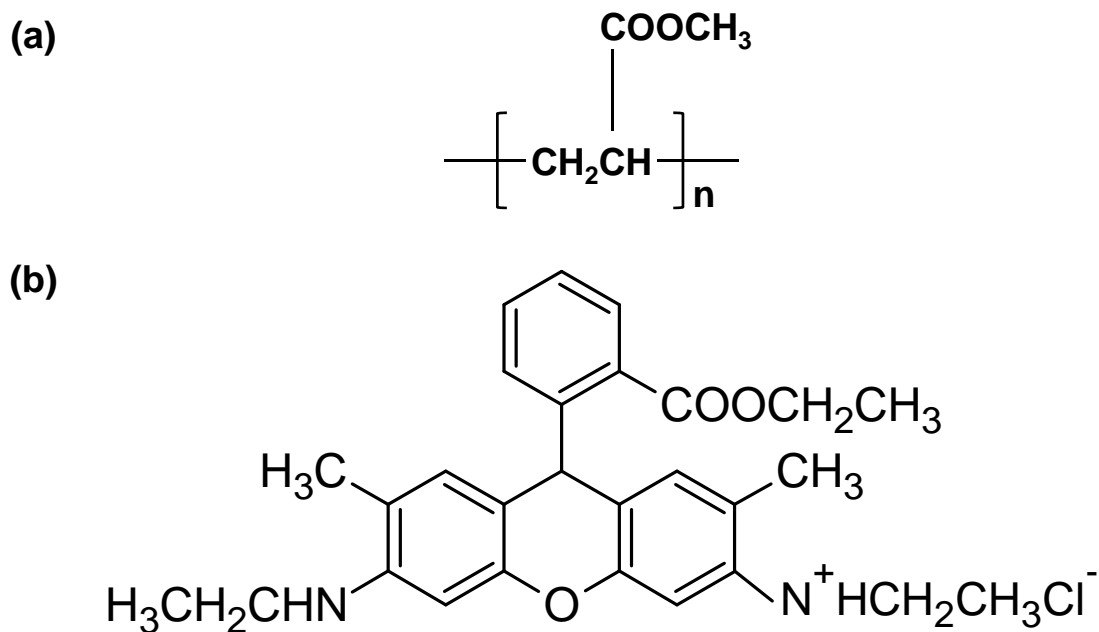
Figure 4.1: The chemical structures of **(a)** poly(methyl acrylate) and **(b)** Rhodamine 6G.

Single molecule experiment was performed using a home-built sample scanning confocal microscope. A simplified schematic diagram of the experimental setup used is shown in figure 4.2. For the purpose of area scanning and moving the excitation beam onto single molecules of R6G, a closed-loop x-y piezo scanning stage (Queensgate, NPS-XY-100A) was used. A laser beam from a 532 nm CW Nd:YAG diode laser (Coherent Laser Division, Model Compass 215M-20) was focused onto the sample using an air-immersion objectives. The numerical aperture (NA) of the objective is 0.6. The excitation beam was modulated to be circularly polarized via 1/4 waveplate to excite single molecules aligned in any directions. Fluorescence of R6G in PMA was collected using the objective again. The fluorescence was filtered by a series of dichroic mirror and 550 longpass filters or 532 notch filter to completely remove the excitation light. Filtered fluorescence was collected by two single photon counting avalanche photodiodes (APD, PerkinElmer Optoelctronics, SPCM-AQR-WX-FC) following being splitted into two orthogonal polarizations using a cube beamsplitter. Vertically polarized fluorescence goes to the APD on right side and horizontally polarized one to the APD on rear side. Two detectors are located on the right angle between each other. Two resulting beams were imaged on the active area of APD. Data collection and sample scanning were controlled using a programmed Labview (National Instruments) program. In order to minimize possible background noise from scattering light, most part of the setup except for the laser was built inside an enclosed box.
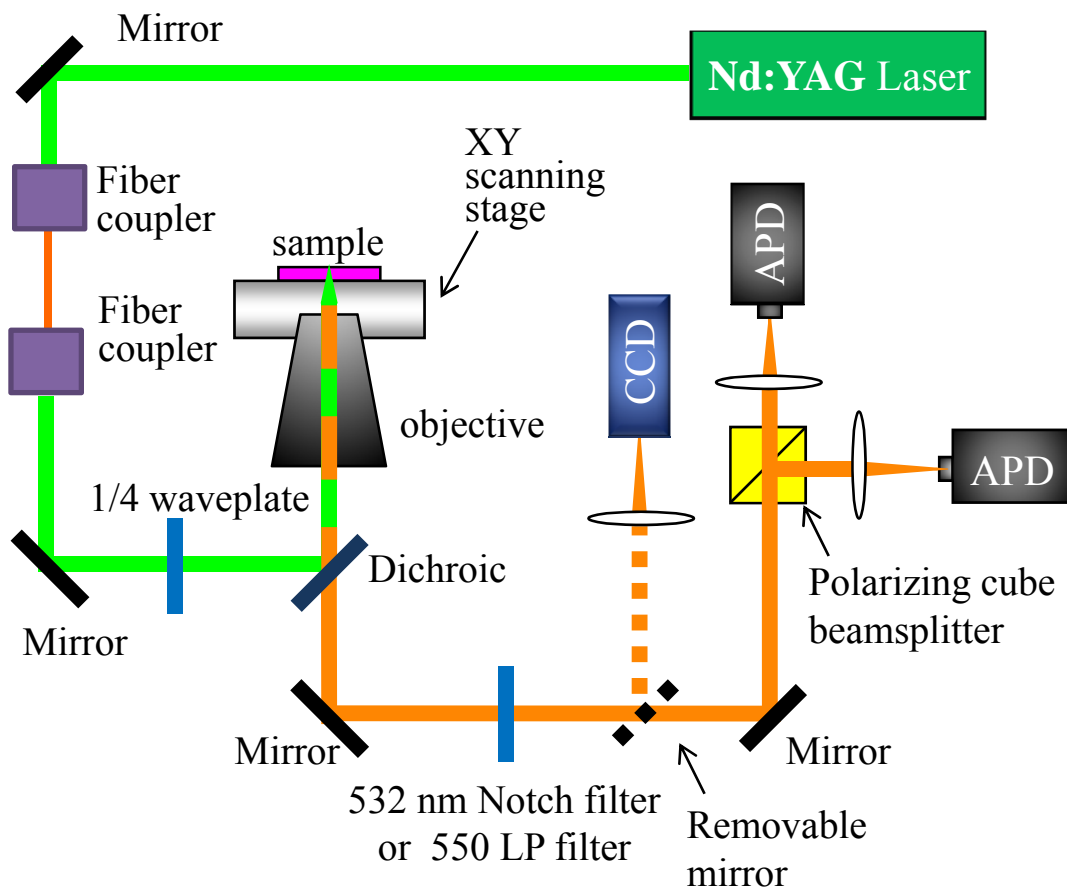
Figure 4.2: A simplified schematic diagram of single molecule experimental setup. A CCD camera is set inside the box to visualize the focal shape of excitation laser beam on the top of the sample film and the image is display in a CRT monitor.

Data Analysis

As a result of rotation of single probe molecules in polymer matrix above glass transition temperature, polarized signals in two orthogonally positioned APD displays anti-correlation in their signal intensities, which represents the rotation of single molecules. In order to compare rotational motion of one single molecule with the rotational motion of other single molecules, quantification of rotation of each molecule was tried. Raw data of two polarized fluorescence signals with respect to time is a three-dimensional data. It is useful to process data if the dimension of data could be reduced. Reduced linear dichroism is the difference of signal intensities normalized by the sum of intensities, which can be calculated using the equation below:

$$A(t) = \frac{I_{//}(t) - I_{\perp}(t)}{I_{//}(t) + I_{\perp}(t)} \qquad \text{(Eq. 4.1)}$$

, where $A(t)$ is a reduced linear dichroism, $I_{//}(t)$ a fluorescence intensity in parallel polarization, $I_{\perp}(t)$ a fluorescence intensity in perpendicular direction. Calculating reduced linear dichroism has an effect of reducing the dimension of data, but still containing the information of rotation.

$$A(t) = \cos 2\theta(t) = \cos 2 \left(\tan^{-1} \sqrt{\frac{I_{//}(t)}{I_{\perp}(t)}} \right) \qquad \text{(Eq. 4.2)}$$

In addition, because of the normalization, it removes any artifacts which may contribute errors to final results, such as laser power fluctuation, signal noise, any

70

unwanted photochemistry like blinking, and so on. Ideally, the reduced linear dichroism, $A(t)$, has a value ranging from +1 to -1. When $A(t)$ is +1, it implicates that the polarization of fluorescence is parallel. As the polarization of the fluorescence is parallel to the dipole moment of dye molecule, it also implies that the molecule is aligned in parallel direction. On the other hand, if $A(t)$ is -1, the molecule is aligned in the perpendicular direction. However, it is not valid in an experiment where signals are collected through a high numerical aperture objective, which is discussed in the previous chapter.

Rotation of single molecules still needs to be quantified more precisely than calculating reduced dichroism for rigorous comparison. As rotation of single molecule is monitored as a function of time, the reduced linear dichroism is also time domain data. Autocorrelation function can find repeating patterns in signals, such as determining the presence of a periodic signal buried under noise, or identifying the missing fundamental frequency in a signal implied by its harmonic frequencies.[33] Therefore, autocorrelation function of reduced dichroism is used to scale rotation of single molecules and enable comparison by estimating rotational time constants. Autocorrelation function of a time domain data can be calculated using following equation:

$$C(t) = \langle A(t')A(t'+t)\rangle = \frac{\sum_{t'=0}^{T} A(t')A(t'+t)}{\sum_{t'=0}^{T} A(t')A(t')} \qquad \text{(Eq.4.3)}$$

, where $C(t)$ is a correlation function a time series, $A(t')$ a time domain data, and $A(t'+t)$ a time domain data at time t'. Autocorrelation function is a measure how

well time domain data $(A(t'))$ matches to its time-shifted version $(A(t' + t))$. In other words, it is a cross-correlation of a data with itself. If t' is zero, the data is perfectly in-phase with its time-shifted data, $C(t)$ has a value of 1. But, if t' increases, phase mismatch increases and $C(t)$ becomes zero. In the analysis of polarized fluorescence signals, it is useful to determine hidden repeating patterns of signals, i.e. rotation of single molecules. Autocorrelation function generally has a form of an exponential decaying from 1 to 0. Therefore, autocorrelation function of the signals can be quantified and ready for comparison to one another by fitting it to a stretched exponential function, also known as Kohlrausch-Williams-Watts (KWW) function:[34]

$$C(t) = \exp\left(-\frac{t}{\tau_{KWW}}\right)^{\beta} \qquad \text{(Eq. 4.4)}$$

, where τ_{KWW} is a rotational time constant, and β a stretching exponent. If β is 1, exponentiality is conceived in rotational dynamics of single molecule, while nonexponentiality better describes the rotational dynamics of the single molecules, if not. These two fitting parameter are very useful in determining and comparing the rotation of single molecules.

RESULTS & DISCUSSIONS

After scanning the sample using x-y scanning stage and directing polarized fluorescence signals into two APDs, two orthogonally polarized fluorescent images

72

are obtained and examples are shown in figure 4.3. Each bright spot in the images corresponds to R6G dye molecules because PMA itself is not fluorescent by 532 nm excitation. Some of bright spots in the images were taken to collect fluorescence signals and check single-step photobleaching (Figure 1.2) as a tool of confirming if they are one single dye molecules. Image displays well separated single probe dyes. Some dyes aggregated one another to make themselves bigger than other spots, which are excluded in data analysis. Any photochemistry such as photobleaching and photoblinking makes variety of fluorescence images of single dyes. The photochemistry and dynamics of single molecules account for the oddity of bright spots such as stripes and half-circle shapes in the images. The size of the image of single dye molecule cannot be smaller than the size of the laser focus because of diffraction limit of light.[35]

Therefore, the size of the fluorescence images of single molecules is about submicron order and determined by convolution of the actual size of the molecules and the size of the laser focus which is defined by following equation[36]:

$$d = \frac{\lambda}{2n \sin \alpha} = \frac{\lambda}{2\text{NA}}. \qquad \text{(Eq. 4.6)}$$

, where d is a diameter of laser focus, λ a wavelength, n refractive index of medium, and NA stands for a numerical aperture of objective. Using 532 nm as an excitation, the sizes of bright spots in the images are about 600-700 nm in diameter.
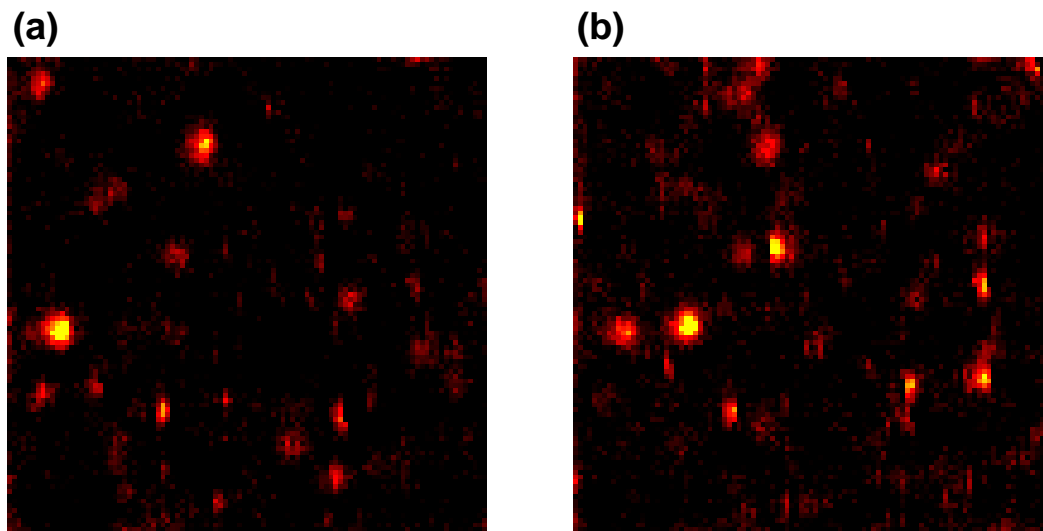
Figure 4.3: Examples of microscopic fluorescence images of single R6G dyes embedded in PMA matrix at 23°C. The concentration of R6G in PMA solution was about 0.1 nM and laser power was maintained below a few nW. The images consist of 100×100 pixels and each step size is 100 nm, which makes the image size shown 10×10μm. Polarized signals are collected by different APDs to display images in **(a)** *s*-polarization and **(b)** *p*-polarization.

Laser focus is placed on each single molecule to collect time transients of fluorescence signals and they are recorded with respect to time using two APDs. A typical example of time transients of fluorescence signals of single dye molecule is shown in figure 4.4(a). As the orientation of transition dipole moment of single molecule is parallel to the polarization of fluorescence, the change of intensities in polarized fluorescence implicates that the single molecule rotates, or accurately speaking, the transition dipole moment of single molecule rotates. As a well-defined orientation of single molecules makes the fluorescence image of the molecule dark in the image of one polarization and bright in the image of other polarization, the same results are valid in time transient data.
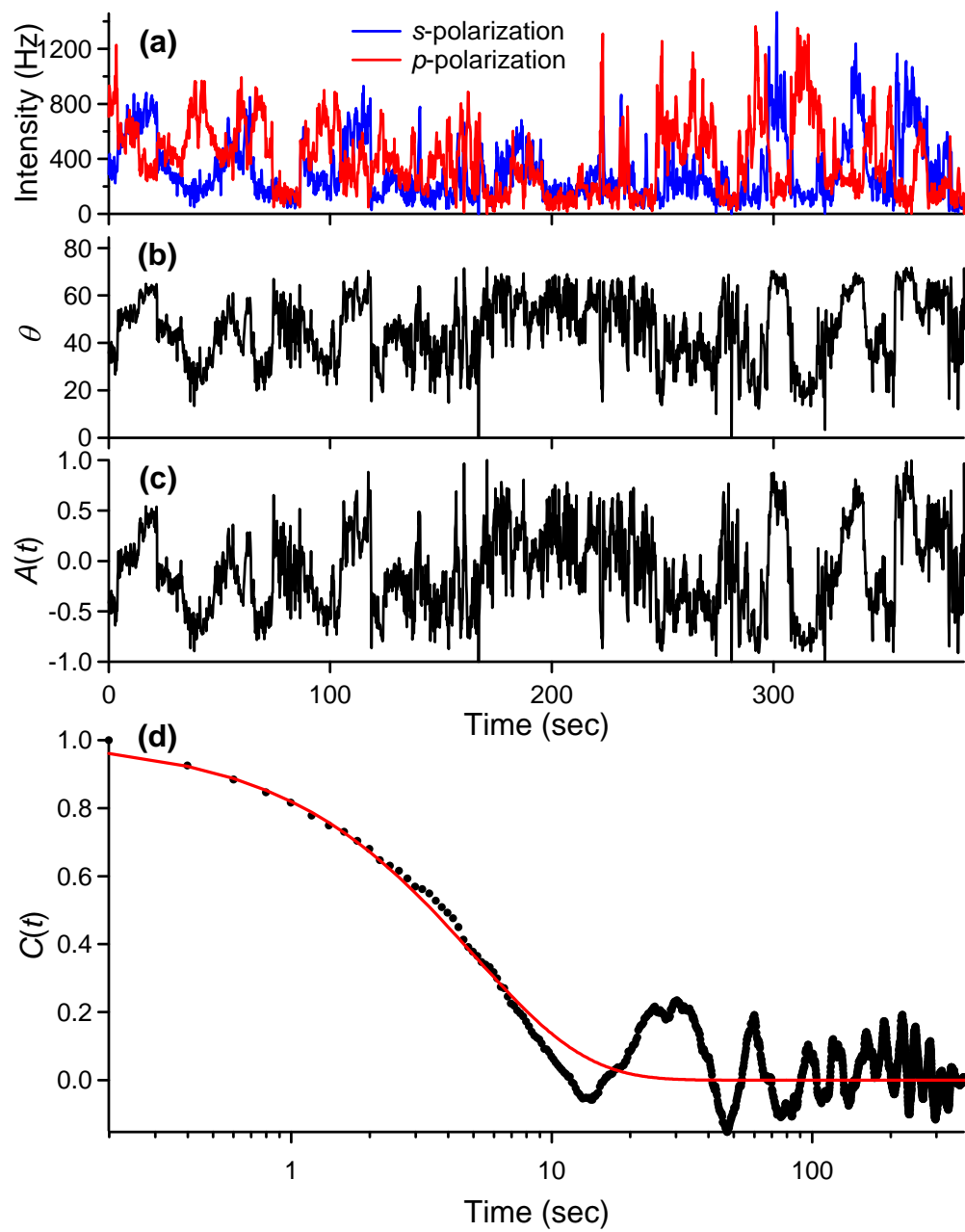
Figure 4.4: An example of data analysis from raw data to correlation function. **(a)** Time transients of fluorescence signals from one single probe molecule, **(b)** rotational angle, **(c)** reduced linear dichroism, and **(d)** calculated correlation function and fitted stretched exponential function.
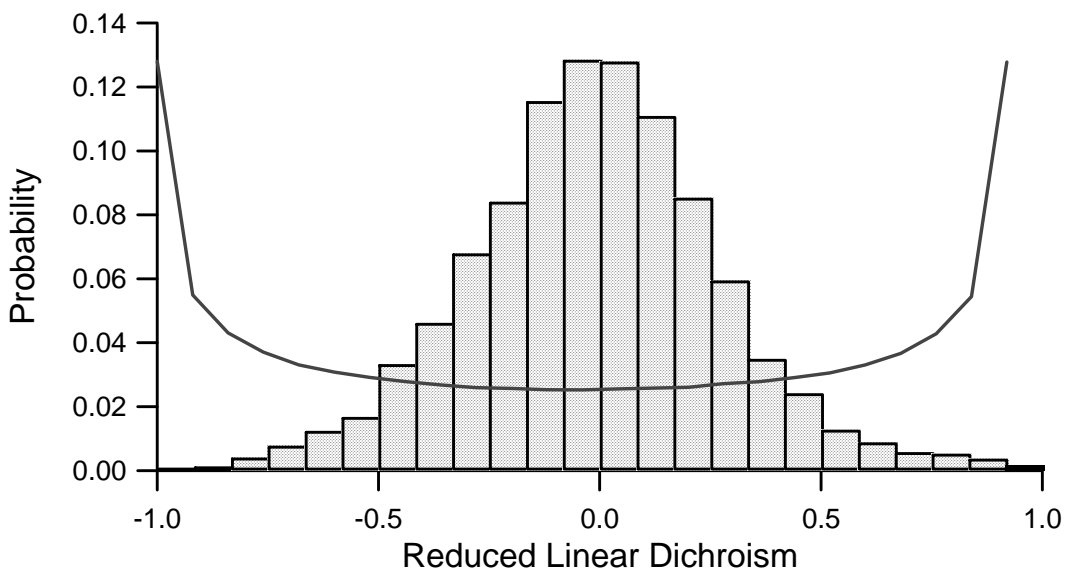
Figure 4.5: Histogram of reduced linear dichroism. Experimental results collected using 1.25 NA objective are shown in bar. Theoretical results calculated using (Eq. 4.2) and assumption of zero NA are shown in solid line for comparison.

If dipole moment is aligned in perpendicular direction, the fluorescence intensity will be at maximum in a detector in perpendicular direction, but at minimum at a detector in parallel direction, or vice versa. Therefore, anticorrelation in two intensities shows another evidence of single molecules rotating around the axes. These intensity changes can be interpreted to rotational information of single molecules. Rotational angle, θ, or angle of a dipole moment projected on the plane perpendicular to the objective axis, is calculated using the (Eq.4.2) and reduced linear dichroism, $A(t)$, calculated using (Eq.4.1), which are shown in figure 4.4(b) and (c). Theoretical estimate of $\cos 2\theta(t)$ is obtained using random walk simulation and its distribution is compared with the experimental distribution of reduced linear dichroism of all

single molecules we collected in this study in figure 4.5. As clearly stated in (Eq. 4.2), cosine value of $2\theta(t)$ is expected to be equal to $A(t)$. The theoretical distribution of reduced linear dichroism is maximized at the limit of ±1, which means the dipole moment is perfectly oriented either in parallel (+1) or perpendicular (-1) direction. However, the experimental distribution does not reach its maximum at the value of ±1 because polarizing effects from the high numerical aperture (NA) objective[37] do not give zero intensity on one polarization at any given dipole orientation. Instead, the experimental reduced linear dichroism shows the most probable values near at zero, which means that the dipole moments of single molecules are aligned nearly along the axis of the objective to have same intensities of projections onto two orthogonal detection axes. As an NA is defined as the following equation:

$$\text{NA} = n \sin \alpha, \qquad\qquad\qquad (\text{Eq. 4.6})$$

a high NA of a objective implies that α approaches to right angle to collect more light from samples with given refractive index of a medium, n. In order to take into consideration of the high NA effect on collecting fluorescence, the (Eq. 4.2) can be corrected into the equation below:

$$A(t) = \frac{C \sin^2 \varphi \cos 2\theta}{A + B \sin^2 \theta}, \qquad\qquad (\text{Eq. 4.7})$$

, where A, B, C are constants defined by NA and n, and φ is defined by the angle between the axis of the objective and dipole moment of single molecules.[38] According to the definitions, (Eq. 4.7) is easily reduced to (Eq. 4.2) when NA of

objective is zero, which is only hypothetical. Using the expression of correlation function, $C(t)$ in terms of spherical harmonics function (Eq. 4.8)[39] invoked in the work of Hinze *et. al.*,[40] the effect of high NA was revisited using 3D simulation of random work in the work of Wei *et. al.*[41]

$$C(t) = \sum_l a_l C_l(t) \qquad \text{(Eq. 4.8)}$$

$$\begin{cases} C_l(t) = e^{-l(l+1)Dt} \\ a_l = \frac{1}{4\pi} \sum_m \left| \int_0^{2\pi} d\theta \int_0^{\pi} d\varphi \sin\varphi \, A(\varphi,\theta) Y_{l,m}(\varphi,\theta) \right|^2 \end{cases}$$

In their work, the label of Legendre polynomial, l, was expanded from 2 to 20 and the estimated value of its corresponding coefficient, a_l, was plotted in terms of different NAs. The simulation clearly showed significantly decreasing contribution from high order term, as the NA increases. The results also displayed zero-peaked histogram of reduced linear dichroism when high NA was considered, which accounts for the discrepancy in figure 4.5.

As the final step of data analysis, correlation function of reduced linear dichroism, $C(t)$, is calculated using (Eq. 4.3) and shown in figure 4.4(d). The fitting parameter β and τ are estimated by fitting correlation function to a stretched exponenetial function (Eq. 4.4). The results of β and τ are found to be very sensitive to a fitting method such that the interpretation of dynamics of single molecule varies dramatically conditions of constraints.[42] In this data analysis, the amplitude of fitting function needs to be fixed at 1, because the first data point of an

ideal correlation function is 1 because of normalization. The condition of β is also a matter of importance in fitting results. In the original physical meaning, $\beta = 1$ represents a homogeneous dynamics upon using the stretched exponential to describe dynamics. Therefore, the condition of β needs to be set between 0 and 1, i.e. $0 < \beta \leq 1$. However, statistically speaking, β dosen't need to be constrained within unity. In fact, β can be greater than 1 because of statistical fluctuation. The only difference of confinement of $\beta \leq 1$ is the results that all β values greater than 1 would be set equal to 1 in fitting process. As a results of these consideration, the confinement of $0 < \beta \leq 1$ is used to fit experimental correlation function to a stretched exponential function. The fitting range is also restricted to time lag q, not the whole range, because the correlation function is basically zero after a certain time lag of q.[43]

In this work, polarized Time transients of fluorescence were collected for analysis from 69 single R6G molecules in PMA film at room temperature of 23 ºC. Correlation functions of reduced linear dichroism of each single molecule was analyzed and fitted to the stretched exponential as described above. The resultant distributions of histogram of a rotational time constant, τ, and a stretching exponent, β from (Eq. 4.4) are plotted in figure 4.6. The average values of 69 single molecules are $<\tau>$=36.23 sec and $<\beta>$=0.71, when fitted to time lag q and β is constrained between 0 and 1. As shown in figure 4.6, the histograms have a distribution rather than fixed at a certain value. However, the distribution of τ is very narrow and maily distributed near the values of between 0 and 30 and the distribution above it is rather negligible. Meanwhile, β has a little broader distribution ranging from single exponential decays to highly non-exponential decays.
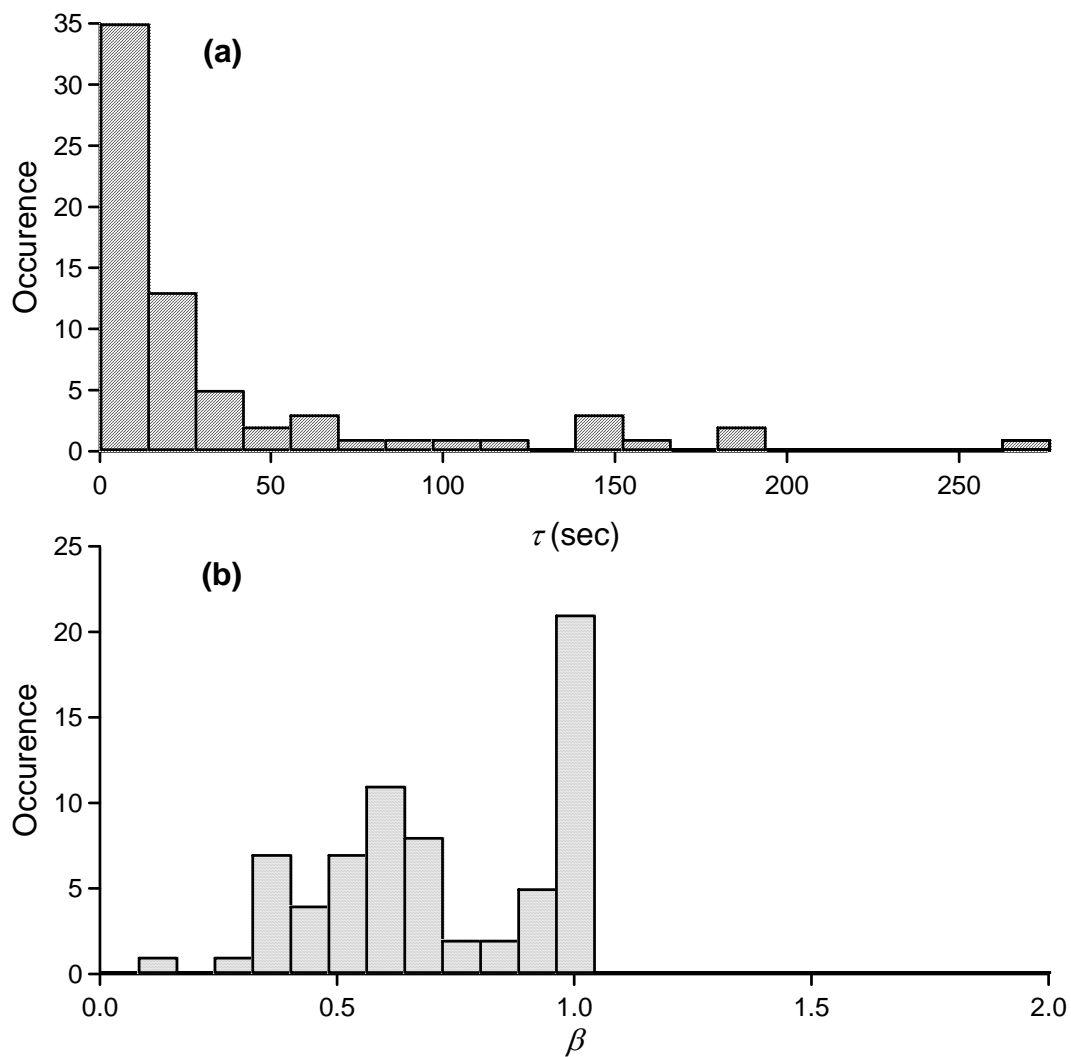
Figure 4.6: The distribution of **(a)** τ and **(b)** β of a set of transients of 69 single molecules in PMA at 23 °C. $<\tau>$=36.23 sec and $<\beta>$=0.71.

However, the value of β is more heavily distributed near at the limit of 1. These results of τ and β suggest that the rotational dynamics of R6G in PMA film at room temperature is fast and it is well supported by the glass transition temperature of PMA well below the room temperature.[14,21-23] As explained in the chapter 1, the dynamics of normal liquid is faster than that of supercooled liquid and expected to exhibit more single exponential decay of the dynamics as the temperature increases. The rotational dynamics measured in this experiment shows mostly single exponential decay and faster dynamics. It means less glassy and viscous state of PMA and simple dynamics in the given conditions. In the work done by Lu and Vanden Bout,[42,44] however, the existence of a "natural distribution" in time constants and stretched exponents was shown even in simulated isotropic rotational diffusion. Single molecule measurement conceives well specifically defined local information. However, as even single molecule measurement cannot avoid the inherent time-averaging, they concluded that the finiteness of single molecule trajectory causes the variance of correlation function. Therefore, if the correlation function is fitted to any model function such as the stretched exponential in this study, the variance of correlation function results in propagating into fitting parameters in consequences. This explains that the distribution of τ and β comes from a finite trajectories of single molecules. Lu and Vanden Bout also suggested that the trajectory length need to be more than 1000 time of time constant to reasonably represent the true value of fitting parameters, which implies the limitation of single molecule spectroscopy. Actually, most of the fluorescence transients of single R6G molecules embedded in PMA film had a range from a few times to 10 times of their rotational constants in length.

81

Their work also provides a key to answer the other question about polymer dynamics in supercooled liquid phase: "Heterogenous Dynamics" vs. "Homogeneous Dynamics". When the rotational dynamics of all single molecules are homogeneous, a single exponential decay of correlation function can be a good proof of homogenous dynamics. When the rotational dynamics of all single molecules are heterogeneous, a non-exponential decay of correlation function will be observed from measurement. However, the assumption doesn't necessarily hold validity in the opposite way. In other words, when non-exponential decay of correlation function of single molecule is measured, it doesn't result in the conclusion of heterogeneous dynamics of single molecules. The inevitable statistical errors of data analysis in single molecule experiment are one of the reasons. As shown in the previous work of Lu and Vanden Bout, finite trajectory could yield non-exponentiality despite homogeneous dynamics only because of limited data sampling. In addition, as the limited data sampling, which cannot be avoided in real experiment in lab, produces distributions of fitting parameters, determination if a system is homogeneous or heterogeneous should be put off until more rigorous statistical analysis is done.

CONCLUSIONS

Polarized fluorescence of R6G in PMA film was investigated and analyzed for single molecule spectroscopy of rotational dynamics of probe molecules in polymer film. Polarized fluorescence signal were easily transformed into a reduced linear dichroism perceiving information of rotation. Autocorrelation of the reduced linear dichroism enables the quantification and comparison of rotation of each single

molecule possible by fitting them to a stretched exponential function, i.e., Kohlrausch-Williams-Watts (KWW) function. As single exponential decay of correlation function of measured reduced linear dichroism implicates the pure rotation of dipole moments of single probe molecules occurs in the matrix of study, the non-exponential decay suggests more complex dynamics. As a result of analysis of fluorescence time transients of 69 single R6G molecules in PMA films at room temperature, the average values of time constant and stretching exponent are $<\tau>$=36.23 sec and $<\beta>$=0.71. When examined by the distribution of the fitting parameters, most of single molecules have time constant ranging between 0 to 30 and stretching exponent mainly distributed near the limit of unity. As the temperature of the sample is well above the glass transition of PMA, the majority of single molecules observed exhibit single exponential decay of homogeneous dynamics. However, both time constants and stretched exponents have distributions, which possibly imply the heterogeneous dynamics.

If the rotational diffusion of PMA is homogeneous, a single exponential correlation function will be yielded with the values of 1 of stretched exponents. But, it needs to be reminded that non-exponential decay is not necessarily lead to the proof of heterogeneous environment. As discussed in the work of Wei *et. al.*,[41] isotropic rotational diffusion didn't result in the single exponential day of correlation function with consideration of high NA effects. The work of Lu and Vanden Bout[42] also provides important evidence to support this manifest. In their analysis of single molecule transients, it was well illustrated that intrinsic statistical errors exist in the single molecule data analysis because of propagation of variance of correlation

83

functions, which stems from time-averaging. It was also shown that the limit of finite data introduces in non-exponential decay of dynamics.

In conclusion, it is unarguably true that the average of single molecule data can be compared to the ensemble average to probe similar environment. However, it needs extra caution when time-averaged results of single molecules are in comparison. It is possible that heterogeneous non-exponentiality of single molecule properties stems from either from real heterogeneity or from limit of data smapling. In order to make a more decisive conclusion in the study of single molecule dynamics, longer transients length, more single molecules, and more decisive statistical test will be required. The distribution should be closely examined and compared to the natural error introduced by statistical fluctuation of limit of raw experimental data before reaching the conclusion of heterogeneity. This conclusion will hold fair validity in all other single molecule experiments.

REFERENCES

(1)   Ediger, M. D. *Ann. Rev. Phys. Chem* **2000**, *51*, 99.

(2)   Ediger, M. D.; Angell, C. A.; Nagel, S. R. *J. Phys. Chem.* **1996**, *100*, 13200.

(3)   Lubchenko, V.; Wolynes, P. G. *Annu. Rev. Phys. Chem.* **2007**, *58*, 235.

(4)   Phillips, J. C. *Rep. Prog. Phys.* **1996**, *59*, 1133.

(5)   Sillescu, H. *J. Non-Cryst. Solids* **1999**, *243*, 81.

(6)   Angell, C. A. *Science* **1995**, *267*, 1924.

(7)   Stillinger, F. H. *Science* **1995**, *267*, 1935.

(8)   Adam, G.; Gibbs, J. H. *J. Chem. Phys.* **1965**, *43*, 139.

(9)   Harrison, G. *The Dynamic Properties of Supercooled Liquids*; Academic Press: New York, 1976.

(10)   Arbe, A.; Colmenero, J.; Monkenbusch, M.; Richter, D. *Phys. Rev. Lett.* **1998**, *81*, 590.

(11)   Cicerone, M. T.; Blackburn, F. R.; Ediger, M. D. *Macromolecules* **1995**, *28*, 8224.

(12)   Cicerone, M. T.; Ediger, M. D. *J. Chem. Phys.* **1995**, *103*, 5684.

(13)   Floudas, G.; Mierzwa, M.; Schonhals, A. *Phys. Rev. E* **2003**, *67*, 031705.

(14)   Floudas, G.; Mpoukouvalas, K.; Papadopoulos, P. *J. Chem. Phys.* **2006**, *124*, 074905/1.

(15)   Glotzer, S. C.; Jan, N.; Lookman, T.; MacIsaac, A. B.; Poole, P. H. *Phys. Rev. E* **1998**, *57*, 7350.

(16)   Sanchis, A.; Prolongo, M. G.; Masegosa, R. M.; Rubio, R. G. *Macromolecules* **1995**, *28*, 2693.

(17)   Heuer, A.; Spiess, H. W. *Phys. Rev. Lett.* **1999**, *82*, 1335.

(18)   Brown, R. *Phil. Mag.* **1828**, *4*, 161.

(19)   Maret, G.; Wolf, P. E. *Z. Phys. B: Condens. Matter* **1987**, *65*.

(20)   Schmidt-Rohr, K.; Spiess, H. W. *Phys. Rev. Lett.* **1991**, *66*, 3020.

(21)   Lu, X. Y.; Jiang, B. Z. *Polymer* **1991**, *32*, 471.

(22)   Soldera, A.; Metatla, N. *Phys. Rev. E* **2006**, *74*, 061803/1.

(23)   Camacho-Zuniga, C.; Ruiz-Trevino, F. A. *Ind. Eng. Chem. Res.* **2003**, *42*, 1530.

(24)   Wang, C.-Y.; Eidger, M. D. *J. Phys. Chem. B* **1999**, *103*, 4177.

(25)   Wang, C.-Y.; Ediger, M. D. *J. Chem. Phys.* **2000**, *112*, 6933.

(26)   Richert, R. *J. Phys.: Condens. Matter* **2002**, *14*, R703.

(27)   Simdyankin, S. I.; Mousseau, N. *Phys. Rev. E* **2003**, *68*, 041110.

(28)   Moerner, W. E.; Fromm, D. P. *Rev. Sci. Instrum.* **2003**, *74*, 2597.

(29)   Weiss, S. *Science* **1999**, *283*, 1676.

(30)   Xie, X. S.; Trautman, J. K. *Annu. Rev. Phys. Chem.* **1998**, *49*, 441.

(31)   Rosenberg, S. A.; Quinlan, M. E.; Forkey, J. N.; Goldman, Y. E. *Acc. Chem. Res.* **2005**, *38*, 583.

(32)   Plakhotnik, T.; Donley, E. A.; Wild, U. P. *Annu. Rev. Phys. Chem.* **1997**, *48*, 181.

(33)   Priestley, M. B. *Spectral analysis and time series*; Academic Press: London, New York, 1981.

(34)   Williams, G.; Watts, D. C.; Dev, S. B.; North, A. M. *Trans. Faraday Soc.* **1971**, *67*, 1323.

(35)   Abbe, E. *Arch. Mikrosk. Anat.* **1873**, *9*, 413.

(36)   Born, M.; Wolf, E.; Bhatia, A. B. *Principles of Optics : Electromagnetic Theory of Propagation, Interference and Diffraction of Light*, 7th ed.; Cambridge University Press: Cambridge[England], New York, 1999.

(37)   Morishita, H.; Hoshino, Y.; Higuchi, S.; Kaneko, F.; Tashiro, K.; Kobayashi, M. *J. Raman Spectrosc.* **2000**, *31*, 455.

(38)   Fourkas, J. T. *Opt. Lett.* **2001**, *26*, 211.

(39)   Berne, B. J.; Pecora, R. *Dynamics Light Scattering*; Dover: Mineola, N.Y., 2000.

(40)   Hinze, G.; Diezemann, G.; Basché, T. *Phys. Rev. Lett.* **2005**, *93*, 203001.

(41)   Wei, C.-Y. J.; Kim, Y. H.; Darst, R. K.; Rossky, P. J.; Vanden Bout, D. A. *Phys. Rev. Lett.* **2005**, *95*, 173001.

(42)   Lu, C.-Y.; Vanden Bout, D. A. *J. Chem. Phys.* **2006**, *125*, 124701.

(43)   Box, G. E. P.; Jenkins, G. M. *Time Series Analysis Forecasting and Control*; Holden-Day: San Francisco, 1970.

(44)   Wei, C.-Y. J.; Lu, C.-Y.; Kim, Y. H.; Vanden Bout, D. A. *J. Fluoresc.* **2007**, *17*, In press.

Appendix A

THE IGOR PROCEDURE FOR IMPORTING A BINARY WINSPEC FILE INTO

```
#pragma rtGlobals=1                    // Use modern global access method.

//Load all files in directory
Macro LoadPrincetonSPEdir()
        String Pathname=""         ,    filename
        Variable index = 0

        if (strlen(pathname) == 0)         //if no path specified, create one
                NewPath /O temporaryPath        //this will put up a dialog
                pathname="temporaryPath"
        endif

        do      // loop through each file in folder
                filename = IndexedFile($pathname, index, ".spe")
                if (strlen (filename) == 0)      //no more files?
                        break                                            //break out of
loop
                endif

                LoadPrincetonSPE(pathName,filename) // Change this procedure for other
filetypes

                index += 1
        while (1)

        if (Exists("temporaryPath"))
                KillPath temporarypath
        endif
End

// General load routine for Princeton binary files as written by e.g. Winspec
// Code based on
//http://www.sccs.swarthmore.edu/users/03/roban/temperature/conversion/read_princeton.pro
// Reads both graphs and images
// Should work with all datatypes, but only type 3 (int) has been tested
// Info from the 4100 byte header is processed and stored in wave notes
// If there is calibration info available, a scaling wave is created
// Optionally, a visible wavelength (nm) can be provided
// to convert scaling to raman shift (cm-1)
// E.g. call this function as LoadPrincetonSPE("", "", vis=800.8)
// Allows for 3D image stacks (e.g. time series)
```

```
Function LoadPrincetonSPE(pathname, filename, [vis])
        string pathname, filename
        variable vis

        variable refnum, tmp, i
        variable exp_sec
        variable nx, ny, nframes, datatype
        string wname, wnameX, wnameY
        string datestr, timestr, comment1, comment2, comment3, comment4, comment5
        string notestr, wavenote=""

        //Open/R/T=".spe" refnum as filename
        open/r/p=$pathname/Z=2/M="Press cancel if you're finished"/t=".spe" refnum as
filename
        if (V_flag<0)
                    abort
        endif

        //Build wavenames
        FStatus refnum
        wname=S_fileName[0,((strlen(S_fileName)-1)-4)]    // remove last 4 chars from
filename
        wname = Cleanupname(wname,0)
        wnameX = wname+"_X"
        wnameY = wname+"_Y"
        Killwaves/Z $wname, $wnameX, $wnameY


        //header info
        FSetPos refnum, 10;             FBinRead/B=3/F=4 refnum,exp_sec //exposure in
seconds
        FSetPos refnum, 42;             FbinRead/B=3/F=2 refnum, nx             //number of x
pixels
        FSetPos refnum, 656;        FbinRead/B=3/F=2 refnum, ny
        //number of y pixels (=1 for graph)
        FSetPos refnum, 1446;     FbinRead/B=3/F=3 refnum, nframes     //number of frames
        FSetPos refnum, 108;        FbinRead/B=3/F=2 refnum, datatype
        //data type float, long, uint, int
        //Date-time
        FSetPos refnum, 20;             FReadLine/N=10 refnum, datestr
        //format DDMMMYYYY (20Apr2005)
        FSetPos refnum, 172;        FReadLine/N=6 refnum, timestr //format HHMMSS
(161959)
        //User Comments
        FsetPos refnum, 200;                    Freadline refnum, comment1
        FsetPos refnum, 280;                    Freadline refnum, comment2
        FsetPos refnum, 360;                    Freadline refnum, comment3
        FsetPos refnum, 440;                    Freadline refnum, comment4
        FsetPos refnum, 520;                    Freadline refnum, comment5
        //use structures to load calibration data from header
        STRUCT xcal1 xc1
```

89

```
STRUCT xcal2 xc2
STRUCT ycal1 yc1
STRUCT ycal2 yc2
FSetPos refnum, 3000 ;    FBinRead/B=3/F=0 refnum, xc1
FSetPos refnum, 3103 ;    FBinRead/B=3/F=0 refnum, xc2
FSetPos refnum, 3489 ;    FBinRead/B=3/F=0 refnum, yc1
FSetPos refnum, 3592 ;    FBinRead/B=3/F=0 refnum, yc2

Close refnum

switch(datatype)
        case 0:              // float ?

GBLoadWave/O/Q/B=3/S=4100/T={2,4}/U=(nx*ny*nframes)/W=(1)/N=WStemp
(S_path+S_filename)
                break
        case 1:              // long ?

GBLoadWave/O/Q/B=3/S=4100/T={32,4}/U=(nx*ny*nframes)/W=(1)/N=WStemp
(S_path+S_filename)
                break
        case 2:              //unit ?

GBLoadWave/O/Q/B=3/S=4100/T={16+64,4}/U=(nx*ny*nframes)/W=(1)/N=WStemp
(S_path+S_filename)
                break
        case 3:              //originally int, changed to unsigned integer

GBLoadWave/O/Q/B=3/S=4100/T={16+64,4}/U=(nx*ny*nframes)/W=(1)/N=WStemp
(S_path+S_filename)
                break
        default:
                abort "Unknown datatype"
    endswitch

    //rename loaded wave to cleaned-up filename
    Duplicate/O WStemp0, $wname; KillWaves/Z   WStemp0
    WAVE w = $wname

    // redimension and create scaling waves
    if (ny>1)                         // image(stack) file
        if (nframes == 1) // image
            redimension/N=(nx,ny) w
        else // 3D image stack
            redimension/N=(nx,ny, nframes) w
        endif

        if (xc2.polynom_coeff[0] != 0)
           // only create scaling wave, when there are polynomial coefs
                make/N=(nx+1)/O $wnameX
```

```
                        // for image scaling waves need to be 1 point longer
                        WAVE xw = $wnameX
                        make/O/N=6 coefX
                        coefX = xc2.polynom_coeff[p]        // fill with polynomial coefficients
from header
                        xw=poly(coefX,x+1)          // winspec counts pixels starting at 1;
Igor at 0
                        KillWaves/Z coefX
                endif
                if (yc2.polynom_coeff[0] != 0)
                        make/N=(ny+1)/O $wnameY
                        // for image scaling waves need to be 1 point longer
                        WAVE yw = $wnameY
                        make/O/N=6 coefY
                        coefY = yc2.polynom_coeff[p]        // fill with polynomial coefficients
from header
                        yw=poly(coefY,x+1)          // winspec counts pixels starting at 1;
Igor at 0
                        KillWaves/Z coefY
                endif
        else             // graph
                if (xc2.polynom_coeff[0] != 0)
                        make/N=(nx)/O $wnameX
                        WAVE xw = $wnameX
                        make/O/N=6 coefX
                        coefX = xc2.polynom_coeff[p]        // fill with polynomial coefficients
from header
                        xw=poly(coefX,x+1)          // winspec counts pixels starting at 1;
Igor at 0
                        KillWaves/Z coefX
                endif
        endif

        // convert wavelength to SFG, if a vis-wavelength is supplied
        if(ParamIsDefault(vis)==0)
                xw = Wvl2SFG(xw, vis)
                reverse/DIM=0 w, xw        //make sure the waves run from left to right
        endif

        //Store all parameters in wavenote?
        sprintf notestr, "File: %s\r", S_Filename                    ;wavenote+=notestr
        sprintf notestr, "Path: %s\r", S_Path                        ;wavenote+=notestr
        sprintf notestr, "Exposure: %g\r", exp_sec          ;wavenote+=notestr
        sprintf notestr, "Frames: %g\r", nframes                     ;wavenote+=notestr
        sprintf notestr, "Captured: %s %s\r", DateStr, TimeColon(Timestr);
wavenote+=notestr
        sprintf notestr, "Comment: %s -- %s -- %s -- %s -- %s\r",
Comment1,Comment2,Comment3,Comment4,Comment5
        wavenote+=notestr
        Note w, wavenote
```

End

// Calibration structures of .spe binary headers
Structure xcal1
        double offset
        double factor
        uchar current_unit
        uchar reserved1
        uchar string1[40]
        uchar reserved2[40]
        uchar calib_valid
        uchar input_unit
        uchar polynom_unit
        uchar polynom_order
        uchar calib_count
EndStructure

Structure xcal2
        double pixel_pos[10]
        double calib_value[10]
        double polynom_coeff[6]
        double laser_position
        uchar reserved3
        uchar new_calib_flag
        uchar calib_label[81]
        uchar expansion[87]
EndStructure

Structure ycal1
        double offset
        double factor
        uchar current_unit
        uchar reserved1
        uchar string1[40]
        uchar reserved2[40]
        uchar calib_valid
        uchar input_unit
        uchar polynom_unit
        uchar polynom_order
        uchar calib_count
EndStructure

Structure ycal2
        double pixel_pos[10]
        double calib_value[10]
        double polynom_coeff[6]
        double laser_position
        uchar reserved3
        uchar new_calib_flag
        uchar calib_label[81]

92

```
            uchar expansion[87]
EndStructure

Function/S TimeColon(timestr)
        string timestr

        string hh, mm, ss
        hh=timestr[0,1]
        mm=timestr[2,3]
        ss=timestr[4,5]

        return hh+":"+mm+":"+ss
End

// Converts wavelength (nm) to SFG Ramanshift (cm-1)
Function Wvl2SFG(wvl, vis)
        variable wvl, vis
        return 1e7/wvl-1e7/vis
End
```

THE IGOR PROCEDURE FOR FITTING SPECTRUM TO THE MODIFIED FRANCK-CONDON PROGRESSION MODEL

```
# #pragma rtGlobals=1            // Use modern global access method.

//Make a table for summary of fitting
Function summary()
        Variable/G Index
        Make/O/N=100 A0,x0,d0,S0,w0,w1,A1,A2,GArea, HRArea, TLArea, Rel_GArea
        Make/O/T/N=100 Filename
        Edit Filename,A0,A1,A2,S0,x0,w0,d0,w1, HRArea, GArea, TLArea, Rel_GArea
End

//GArea= Area of Green Component
//HRArea=Area of Huang-Rhys Component
//TLArea=Total Area
//Rel_GArea=Relative Area of Green Component
//Fit emission spectrum with the sum of 5 Gaussian Functions//
//Width of each Gaussian is convoluted    with a Gaussian distribution progression in width//

Function GaussSum5_w_S10(w,x) : FitFunc
        Wave w
        Variable x

        //CurveFitDialog/ These comments were created by the Curve Fitting dialog.
        //CurveFitDialog/ Altering them will make the function less convenient to work with
```

```
//CurveFitDialog/ in the Curve Fitting dialog.
//CurveFitDialog/ Equation:
//CurveFitDialog/ f(x) = A1*A0*exp(-0.5*((x-x0)/w0)^2)
                        +A0*exp(-0.5*((x-x0+d0)/(w0^2+w1^2)^0.5)^2)*S0
                        +A0*exp(-0.5*((x-x0+2*d0)/(w0^2+4*w1^2)^0.5)^2)*S0^2/2
                        +A0*exp(-0.5*((x-x0+3*d0)/(w0^2+9*w1^2)^0.5)^2)*S0^3/6
                        +A0*exp(-0.5*((x-x0+4*d0)/(w0^2+16*w1^2)^0.5)^2)*S0^4/24
                        +A2*(0.98269*exp(-0.5*((x-2.2645)/0.20439)^2)
                        +0.30397*exp(-0.5*((x-2.7438)/0.08998)^2))
//CurveFitDialog/ End of Equation
//CurveFitDialog/ Independent Variables 1
//CurveFitDialog/ x
//CurveFitDialog/ Coefficients 8
//CurveFitDialog/ w[0] = A0
//CurveFitDialog/ w[1] = x0
//CurveFitDialog/ w[2] = d0
//CurveFitDialog/ w[3] = S0
//CurveFitDialog/ w[4] = w0
//CurveFitDialog/ w[5] = w1
//CurveFitDialog/ w[6] = A1
//CurveFitDialog/ w[7] = A2

        return w[6]*w[0]*exp(-0.5*((x-w[1])/w[4])^2)
                +w[0]*exp(-0.5*((x-w[1]+w[2])/(w[4]^2+w[5]^2)^0.5)^2)*w[3]
                +w[0]*exp(-0.5*((x-w[1]+2*w[2])/(w[4]^2+4*w[5]^2)^0.5)^2)*w[3]^2/2
                +w[0]*exp(-0.5*((x-w[1]+3*w[2])/(w[4]^2+9*w[5]^2)^0.5)^2)*w[3]^3/6
                +w[0]*exp(-0.5*((x-w[1]+4*w[2])/(w[4]^2+16*w[5]^2)^0.5)^2)*w[3]^4/24
                +w[7]*(0.98269*exp(-0.5*((x-2.2645)/0.20439)^2)
                +0.30397*exp(-0.5*((x-2.7438)/0.08998)^2))
End

Function FGS5_var1(ywave)
        Wave ywave
        Wave A0,x0,d0,S0,w0,w1,A1,A2 // A2 is the amplitude of empirical green
components
        Wave Filename
        Wave PhotonE // in eV
        Wave GArea, HRArea, TLArea, Rel_GArea
        Variable/G index
        String TimeX, DiffX, GRN, GS0, GS1, GS2, GS3, GS4
        Variable/G iA0=1.24,iA1=1.0,iA2=0.0
        Variable/G ix0=2.825
        Variable/G iw0=0.03,iw1=0.02
        Variable/G iS0=0.65
        Variable/G id0=0.15307

//Duplicate raw data and do analysis the copied data
        TimeX=NameofWave(ywave)+"_norm"
        Duplicate/O ywave $TimeX
        Wave imsi1=$TimeX
```

```
        Wavestats/Q imsi1
        imsi1=imsi1/V_max
        Display $TimeX vs PhotonE
        ModifyGraph rgb[0]=(65280,0,65280), mode[0]=2, lsize[0]=2
        SetAxis bottom 1.5,3.3


//Fitting a spectrum to the sum of 5 gaussian functions//
        Make/D/N=8/O W_coef
        W_coef[0] = {iA0,ix0,id0,iS0,iw0,iw1,A1,iA2}
        FuncFit/H="00000010" GaussSum5_w_S10 W_coef    $TimeX[200,1000]
/X=PhotonE /D

//Draw individual gaussian functions on the fitting results//
        GRN=NameofWave(ywave)+"_GRN"
        GS0=NameofWave(ywave)+"_GS0"
        GS1=NameofWave(ywave)+"_GS1"
        GS2=NameofWave(ywave)+"_GS2"
        GS3=NameofWave(ywave)+"_GS3"
        GS4=NameofWave(ywave)+"_GS4"
        Duplicate/O ywave $GRN, $GS0, $GS1, $GS2, $GS3, $GS4 //,$GS5
        Wave GRNF=$GRN
        Wave GSF0=$GS0
        Wave GSF1=$GS1
        Wave GSF2=$GS2
        Wave GSF3=$GS3
        Wave GSF4=$GS4
        GRNF=W_coef[7]*(0.98269*exp(-0.5*((PhotonE-2.2645)/0.20439)^2)
                +0.30397*exp(- 0.5*((PhotonE-2.7438)/0.08998)^2))
        GSF0=W_coef[6]*W_coef[0]*exp(-0.5*((PhotonE-W_coef[1])/W_coef[4])^2)
        GSF1=W_coef[0]*exp(-0.5*((PhotonE-    W_coef[1]+1*W_coef[2])
                /(W_coef[4]^2+W_coef[5]^2)^0.5)^2)*W_coef[3]/1
        GSF2=W_coef[0]*exp(-0.5*((PhotonE-    W_coef[1]+2*W_coef[2])
                /(W_coef[4]^2+4*W_coef[5]^2)^0.5)^2)*W_coef[3]^2/2
        GSF3=W_coef[0]*exp(-0.5*((PhotonE-    W_coef[1]+3*W_coef[2])
                /(W_coef[4]^2+9*W_coef[5]^2)^0.5)^2)*W_coef[3]^3/6
        GSF4=W_coef[0]*exp(-0.5*((PhotonE-    W_coef[1]+4*W_coef[2])
                /(W_coef[4]^2+16*W_coef[5]^2)^0.5)^2)*W_coef[3]^4/24
        AppendToGraph $GS0,$GS1,$GS2,$GS3,$GS4, $GRN vs PhotonE
        ModifyGraph rgb[2]=(0,0,65280),rgb[3]=(0,0,65280),rgb[4]=(0,0,65280)
        ModifyGraph rgb[5]=(0,0,65280),rgb[6]=(0,0,65280), rgb[7]=(0,56000,0)

//Enter fitting results into the summary table//
        A0[index]=W_coef[0]
        x0[index]=W_coef[1]
        d0[index]=W_coef[2]
        S0[index]=W_coef[3]
        w0[index]=W_coef[4]
        w1[index]=W_coef[5]
        A1[index]=W_coef[6]
```

```
        A2[index]=W_coef[7]
```

```
//Area of Gaussian: sqrt(2pi)*Amplitude*Width
        GArea[index]=W_coef[7]*(0.98269*(2*3.151592)^0.5*0.20439
                        +0.30397*(2*3.141592)^0.5*0.0899)
        HRArea[index]=W_coef[0]*W_coef[6]*(2*3.151592)^0.5*(W_coef[4])
            +W_coef[0]*(2*3.151592)^0.5*(W_coef[4]^2+W_coef[5]^2)^0.5*W_coef[3]
            +W_coef[0]*(2*3.151592)^0.5*(W_coef[4]^2+4*W_coef[5]^2)^0.5*W_coef[5]^2/2
            +W_coef[0]*(2*3.151592)^0.5*(W_coef[4]^2+9*W_coef[5]^2)^0.5*W_coef[5]^3/6

        +W_coef[0]*(2*3.151592)^0.5*(W_coef[4]^2+16*W_coef[5]^2)^0.5*W_coef[5]^4/24
        TLArea[index]=HRArea[index]+GArea[index]
        Rel_GArea[index]=GArea[index]/(HRArea[index]+GArea[index])
        index=index+1
```

```
// Calculate the differnce between the experimental spectrum
//and fitting results from 5 Gaussian functions
        DiffX=NameofWave(ywave)+"_diff"
        Duplicate/O $TimeX $DiffX        //Duplicate raw data and do analysis the copied data
        Wave imsi2=$DiffX
        imsi2=imsi2-(GSF0+GSF1+GSF2+GSF3+GSF4)
        AppendtoGraph $DiffX vs PhotonE
        ModifyGraph rgb[8]=(0,52224,0), mode[8]=2, lsize[8]=2
        ModifyGraph standoff(bottom)=0; ModifyGraph standoff(left)=0
        SetAxis left 0,1.1
End
```

```
Function GaussSum5_w_S12(w,x) : FitFunc
        Wave w
        Variable x

        //CurveFitDialog/ These comments were created by the Curve Fitting dialog.
        //CurveFitDialog/ Altering them will make the function less convenient to work with
        //CurveFitDialog/ in the Curve Fitting dialog.
        //CurveFitDialog/ Equation:
        //CurveFitDialog/ f(x) = A1*A0*exp(-0.5*((x-x0)/w0)^2)
                            +A0*exp(-0.5*((x-x0+d0)/(w0^2+w1^2)^0.5)^2)*S0
                            +A0*exp(-0.5*((x-x0+2*d0)/(w0^2+4*w1^2)^0.5)^2)*S0^2/2
                            +A0*exp(-0.5*((x-x0+3*d0)/(w0^2+9*w1^2)^0.5)^2)*S0^3/6
                            +A0*exp(-0.5*((x-x0+4*d0)/(w0^2+16*w1^2)^0.5)^2)*S0^4/24
                            +A2*(0.98269*exp(-0.5*((x-2.2645)/0.20439)^2))
        //CurveFitDialog/ End of Equation
        //CurveFitDialog/ Independent Variables 1
        //CurveFitDialog/ x
        //CurveFitDialog/ Coefficients 8
        //CurveFitDialog/ w[0] = A0
        //CurveFitDialog/ w[1] = x0
        //CurveFitDialog/ w[2] = d0
        //CurveFitDialog/ w[3] = S0
        //CurveFitDialog/ w[4] = w0
```

```
        //CurveFitDialog/ w[5] = w1
        //CurveFitDialog/ w[6] = A1
        //CurveFitDialog/ w[7] = A2

        return w[6]*w[0]*exp(-0.5*((x-w[1])/w[4])^2)
                +w[0]*exp(-0.5*((x-w[1]+w[2])/(w[4]^2+w[5]^2)^0.5)^2)*w[3]
                +w[0]*exp(-0.5*((x-w[1]+2*w[2])/(w[4]^2+4*w[5]^2)^0.5)^2)*w[3]^2/2
                +w[0]*exp(-0.5*((x-w[1]+3*w[2])/(w[4]^2+9*w[5]^2)^0.5)^2)*w[3]^3/6
                +w[0]*exp(-0.5*((x-w[1]+4*w[2])/(w[4]^2+16*w[5]^2)^0.5)^2)*w[3]^4/24
                +w[7]*(0.98269*exp(-0.5*((x-2.2645)/0.20439)^2))

End

//Blue portion of the emipirical Green component is eliminated and used for fitting
Function FGS5_var2(ywave)
        Wave ywave
        Wave A0,x0,d0,S0,w0,w1,A1,A2
// A2 is the amplitude of empirical green components
        Wave Filename
        Wave PhotonE // in eV
        Wave GArea, HRArea, TLArea, Rel_GArea
        Variable/G index
        String TimeX,DiffX ,GRN, GS0, GS1, GS2, GS3, GS4
        Variable/G iA0=1.24,iA1=1.0,iA2=0.048
        Variable/G ix0=2.825
        Variable/G iw0=0.03,iw1=0.02
        Variable/G iS0=0.65
        Variable/G id0=0.15307

//Duplicate raw data and do analysis the copied data
        TimeX=NameofWave(ywave)+"_norm"
        Duplicate/O ywave $TimeX
        Wave imsi1=$TimeX
        Wavestats/Q imsi1
        imsi1=imsi1/V_max
        Display $TimeX vs PhotonE
        ModifyGraph rgb[0]=(65280,0,65280), mode[0]=2, lsize[0]=2
        SetAxis bottom 1.5,3.3

//Fitting a spectrum to the sum of 5 gaussian functions//
        Make/D/N=8/O W_coef
        W_coef[0] = {iA0,ix0,id0,iS0,iw0,iw1,A1,A2}
        FuncFit/H="00000010"   GaussSum5_w_S12 W_coef   $TimeX[200,1000]
/X=PhotonE /D

//Draw individual gaussian functions on the fitting results//
        GRN=NameofWave(ywave)+"_GRN"
        GS0=NameofWave(ywave)+"_GS0"
        GS1=NameofWave(ywave)+"_GS1"
        GS2=NameofWave(ywave)+"_GS2"
```

```
        GS3=NameofWave(ywave)+"_GS3"
        GS4=NameofWave(ywave)+"_GS4"
//      GS5=NameofWave(ywave)+"_GS5"
        Duplicate/O ywave $GRN, $GS0,$GS1,$GS2,$GS3,$GS4 //,$GS5
        Wave GRNF=$GRN
        Wave GSF0=$GS0
        Wave GSF1=$GS1
        Wave GSF2=$GS2
        Wave GSF3=$GS3
        Wave GSF4=$GS4
        GRNF=W_coef[7]*(0.98269*exp(-0.5*((PhotonE-2.2645)/0.20439)^2))
        GSF0=W_coef[6]*W_coef[0]*exp(-0.5*((PhotonE-W_coef[1])/W_coef[4])^2)
        GSF1=W_coef[0]*exp(-0.5*((PhotonE-W_coef[1]+1*W_coef[2])
            /(W_coef[4]^2+W_coef[5]^2)^0.5)^2)*W_coef[3]/1
        GSF2=W_coef[0]*exp(-0.5*((PhotonE-W_coef[1]+2*W_coef[2])
            /(W_coef[4]^2+4*W_coef[5]^2)^0.5)^2)*W_coef[3]^2/2
        GSF3=W_coef[0]*exp(-0.5*((PhotonE-W_coef[1]+3*W_coef[2])
            /(W_coef[4]^2+9*W_coef[5]^2)^0.5)^2)*W_coef[3]^3/6
        GSF4=W_coef[0]*exp(-0.5*((PhotonE-W_coef[1]+4*W_coef[2])
            /(W_coef[4]^2+16*W_coef[5]^2)^0.5)^2)*W_coef[3]^4/24
        AppendToGraph $GS0,$GS1,$GS2,$GS3,$GS4, $GRN vs PhotonE
        ModifyGraph rgb[2]=(0,0,65280),rgb[3]=(0,0,65280),rgb[4]=(0,0,65280)
        ModifyGraph rgb[5]=(0,0,65280),rgb[6]=(0,0,65280), rgb[7]=(0,56000,0)

//Enter fitting results into the summary table//
        A0[index]=W_coef[0]
        x0[index]=W_coef[1]
        d0[index]=W_coef[2]
        S0[index]=W_coef[3]
        w0[index]=W_coef[4]
        w1[index]=W_coef[5]
        A1[index]=W_coef[6]
        A2[index]=W_coef[7]

//Area of Gaussian: sqrt(2pi)*Amplitude*Width
        GArea[index]=W_coef[7]*(0.98269*(2*3.151592)^0.5*0.20439
+0.30397*(2*3.141592)^0.5*0.0899)
        HRArea[index]=W_coef[0]*W_coef[6]*(2*3.151592)^0.5*(W_coef[4])
+W_coef[0]*(2*3.151592)^0.5*(W_coef[4]^2+W_coef[5]^2)^0.5*W_coef[3]
+W_coef[0]*(2*3.151592)^0.5*(W_coef[4]^2+4*W_coef[5]^2)^0.5*W_coef[5]^2/2
+W_coef[0]*(2*3.151592)^0.5*(W_coef[4]^2+9*W_coef[5]^2)^0.5*W_coef[5]^3/6
+W_coef[0]*(2*3.151592)^0.5*(W_coef[4]^2+16*W_coef[5]^2)^0.5*W_coef[5]^4/24
        TLArea[index]=HRArea[index]+GArea[index]
        Rel_GArea[index]=GArea[index]/(HRArea[index]+GArea[index])
        index=index+1
  End

// fitting experimental green emission spectrum of PFO
// using two independent Gaussian Functions
// this function enables to include emprical green components into the whole fitting process
```

```
Function Greenfit(w,x) : FitFunc
        Wave w
        Variable x

        //CurveFitDialog/ These comments were created by the Curve Fitting dialog.
        //CurveFitDialog/ Altering them will make the function less convenient to work
        //CurveFitDialog/ with in the Curve Fitting dialog.
        //CurveFitDialog/ Equation:
        //CurveFitDialog/ f(x) = A4*exp(-0.5*((x-x4)/w4)^2)+A5*exp(-0.5*((x-x5)/w5)^2)
        //CurveFitDialog/ End of Equation
        //CurveFitDialog/ Independent Variables 1
        //CurveFitDialog/ x
        //CurveFitDialog/ Coefficients 6
        //CurveFitDialog/ w[0] = A4
        //CurveFitDialog/ w[1] = x4
        //CurveFitDialog/ w[2] = w4
        //CurveFitDialog/ w[3] = A5
        //CurveFitDialog/ w[4] = x5
        //CurveFitDialog/ w[5] = w5

        return w[0]*exp(-0.5*((x-w[1])/w[2])^2)+w[3]*exp(-0.5*((x-w[4])/w[5])^2)
End

Function GRNFIT (ywave)
        Wave ywave
        Wave PhotonE
        Wave GRN1, GRN2
        Variable/G iA4=0.98,ix4=2.26,iw4=0.20
        Variable/G iA5=0.30,ix5=2.74,iw5=0.09
        Duplicate ywave GRN1,GRN2
        Display ywave vs PhotonE
        ModifyGraph rgb[0]=(65280,0,65280), mode[0]=2, lsize[0]=2

        Make/D/N=6/O W_coef
        W_coef[0] = {iA4,ix4,iw4,iA5,ix5,iw5}
        FuncFit Greenfit   W_coef ywave /X=PhotonE /D

        GRN1=W_coef[0]*exp(-0.5*((PhotonE-W_coef[1])/W_coef[2])^2)
        GRN2=W_coef[3]*exp(-0.5*((PhotonE-W_coef[4])/W_coef[5])^2)

        ModifyGraph rgb[1]=(0,0,0)
        AppendtoGraph GRN1,GRN2 vs PhotonE
        ModifyGraph rgb[2]=(0,0,65280),rgb[3]=(0,0,65280)
End

Function ZeroWave(w)
        Wave w
        w = 0
        Print "Zeroed the contents of", NameofWave(w)
```

```
        Print NameofWave($"")
End
```

Vita

Yeon Ho Kim was born on March 8, 1973 in Daejeon, South Korea as the son of Sung Moon Kim and Mi-Kyung Jung. After graduating from Daesung High School, he entered Seoul National University, Korea majoring in Chemistry in 1992. Meantime, he completed two-and-a-half years of military service in the Korean Army as a chemical specialist. Upon completion of his undergraduate degree in 1998, he started his master's study at the Graduate School of Seoul National and was conferred the Master of Science in Physical Chemistry for the work of the photodissociation mechanism of organic molecules in mass spectrometer in 2001. In the same year, he came to the United States to pursue further studies in physical chemistry at the University of Texas at Austin and joined Professor David A. Vanden Bout. He was married in May of 2006 to Ui Jeong Moon.

Permanent address: Byuksan APT 117-102, Nae-dong, Seo-gu, Daejeon 302-181,
                                       South Korea

This dissertation was typed by Yeon Ho Kim.